Jefferson Lab Technical Note: **JLAB-TN-03-017**

Target Density Fluctuations and Bulk Boiling in the Hall A Cryotarget

D.S. Armstrong[1] , B. Moffit[1] , R. Suleiman[2]

[1] *College of William and Mary*
[2] *Massachusetts Institute of Technology*

May 6, 2003

Abstract

Beam-induced density change ('boiling') was studied in the Jefferson Lab Hall A cryotarget using the machined 'cigar-tube' target cells. Luminosity monitors were used to study both the reduction in the average target luminosity, and the onset of non-statistical fluctuations in the luminosity, as a function of beam current, raster size, fan speed, beam spot size, for both lH_2 and lD_2. New information on the characteristic time scale of the fluctuations was obtained.

1 Introduction

This report summarizes studies of beam-induced density changes in cryogenic targets, using simple luminosity monitors. The Hall A cryotarget was investigated, using target cells of different lengths (4 cm and 15 cm) with liquid hydrogen and deuterium, with a 5.0 GeV electron beam. We have studied both the change in average luminosity due to decreased target density (referred to here as 'bulk effect'), and the non-statistical fluctuations in luminosity on the millisecond time scale (referred to here as 'fluctuations'). The former effect is important for cross section measurements, and, as discussed below, the latter effect is of particular interest to parity-violation experiments using cryotargets. We have studied the effects of varying the beam current, beam raster size and shape, intrinsic beam spot size, and target fan speed, on both the bulk effect and on the fluctuations. The data were obtained Nov. 14, 2002, in a two-shift facility development period just after the end of E01-020. About 90 runs under different conditions were obtained and analyzed. The target cells investigated were all of the standard machined 'cigar-tube' style used in many recent experiments in Hall A and Hall C at Jefferson Lab (see Fig. 1).

2 Motivation

Precision measurements of parity violation in electron scattering from cryotargets (*e.g.*, liquid hydrogen, deuterium, cold gaseous helium) are sensitive to any time-dependent fluctuations in the target density. The experiments measure the helicity-dependent asymmetry in the scattering rate. Typically, the beam helicity is changed every 33 ms, and the asymmetry is formed from the difference in the scattering rate in two consecutive 33 ms windows, divided by the sum. These "window-pair" asymmetries are then averaged over the run to yield the physics asymmetry of interest. Beam current is normalized out in each 33 ms window. If the target density fluctuates from window to window, causing additional fluctuations

Figure 1: Cryotarget cells: machined cylindrical 'cigar-tube' style.

in the scattering rate, the statistical precision of the asymmetry is degraded beyond Poisson counting statistics.

To set the scale of the problem, the detected counting rate per detector in the HAPPEX-I experiment [1] was 1.2 MHz at 100 μA of beam, yielding a counting statistics width (σ) of 3600 ppm (part per million) per window pair. Limits on target density fluctuations under running conditions were set at $<$250 ppm [2], which, added in quadrature, caused negligible worsening of the statistical width. The HAPPEX-II experiment [3] will have a detected rate per detector of about 90 MHz at 100 μA yielding a statistical width of 400 ppm. Thus target density fluctuations of 250 ppm would increase the statistical error by 18% (or increase the running time required to achieve the proposed precision by 39%); fluctuations of 1000 ppm would increase the error by a factor of 2.7, which would be a disaster.

One should note that it is only the fluctuations on the time scale 33 ms that are important; much slower variations will tend to cancel in the pair-differences, and much faster ones will average out over the 33 ms window.

It is also important to note that the fluctuations we are concerned with have nothing to do with the actual beam helicity. Possible false asymmetries due to helicity-correlated target density changes are a different effect, which should be manageable, since the beam current asymmetry (the helicity-correlated difference in beam charge in window pairs) will be controlled to the ppm level. Assuming that the target density decreases by 5% per 100 μA of beam, a "grand-average" 1 ppm beam current asymmetry would lead to a 100 ppb false asymmetry. This is of the same order as our statistical error, however the effect should be able to be regressed out, since there will be large natural variations in the charge asymmetry. The luminosity monitors themselves should also enable the effect to be corrected for. Note that the calculation above likely overestimates the effect, since it assumes that the target "responds" perfectly to beam current differences on time scales short compared to 33 ms, which as well shall see, is probably not correct. Nevertheless, it is clearly desirable to have the bulk effect loss in average density at 100 μA be under 10%.

Finally, the bulk effect also degrades the statistical precision in the ordinary manner, by reducing the counting rate (and is, of course, a significant concern for cross section measurements). But notice that a 10% bulk effect degrades the statistics by 10%; but it only requires 200 ppm fluctuations at 15 Hz to cause the same degradation in statistics.

Many studies of the bulk effect in various target cells have been performed at Jefferson Lab (see Appendix A), but to our knowledge the only previous study of the fluctuations was from the HAPPEX-I experiment [2].

3 Physics of Target Boiling

The physics of target density changes in high-power cryotargets is complex - see [4]. The flow is expected to be highly turbulent, and will possibly vary along the length of the target cell. The local density will change in the liquid phase as it warms, and of course it can boil, causing large local density changes. Boiling, if present, is unlikely to be uniform through the cell, but will likely start at the surfaces of the heated target windows; the rate by which heat is conducted away will depend on whether the boiling at the window is nucleate (bubbles) or makes a transition to film boiling (where the window is in contact with vapor rather than liquid). It is clearly a difficult task to model the short time-scale fluctuations in target density in such a system.

Note that the density changes by 1.5%/K in liquid hydrogen; thus a cell operating at 19 K and 1.5 atm can maintain at most a 4% density change before undergoing a phase transition (boiling point = 21.7 K). We have surveyed target luminosity scan data from Halls A and C taken over the past several years (see Appendix A); they show bulk effect density losses for hydrogen at 100 μA of as small as 2.4% and as large as 20%, depending on cell geometry, raster size and type, target fan speed, and possibly other variables. Clearly, there must be actual boiling in many of these cases. The bulk density *vs.* beam current data are typically consistent with being linear; no sudden onset of boiling is seen.

Target density changes on a microscopic scale should be sensitive to the intrinsic beam spot size, the raster frequency, and the uniformity of the raster pattern; heating on a macroscopic scale should depend primarily on the raster size.

4 Luminosity Detectors

The luminosity monitors used are simple lucite (UVT acrylic, Bicron BC-800) sheets (12 inch long, 2 inch wide, 3/8 inch thick), coupled to cylindrical light guides, and each viewed by a Hamamatsu R329-02 12-stage 2 inch PMT: see Figs. 2, 3, 4. They respond primarily to Cerenkov light, *e.g.*, from electromagnetic showers.

Setup for November 14 2002 test run:

1. Lumi 1 on frame, 7 m downstream of pivot, at 3.2° scattering angle. on the right of the beamline.
2. Lumi 2 on frame, 7 m downstream of pivot, at 3.2° scattering angle, on the left of the beamline.
3. Lumi 3 on pivot, on the left side of beam, with 1 lead brick of shielding on the PMT. The scattering angle was about 27°, and it was located at 1.5 m from target .

The standard square raster was used. **Note**: everywhere in this report, the raster setting is reported, in full width (x) *vs.* full width (y); the actual beam spot dimensions at the target are a factor of 1.4 larger, *i.e.*, a 1.4 mm×1.4 mm setup gives a 2 mm×2 mm spot at the target location.

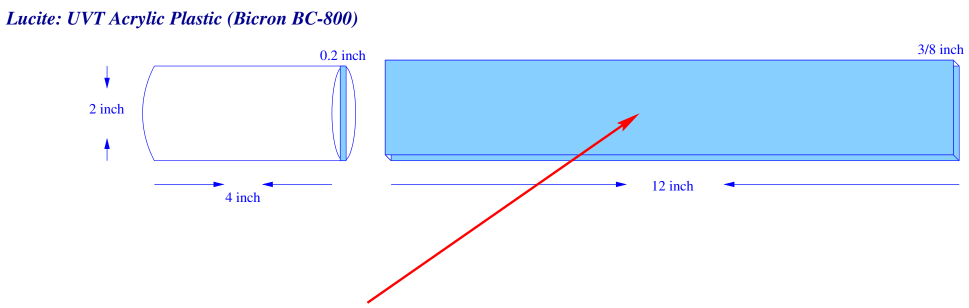

Figure 2: Lumi detector schematic.

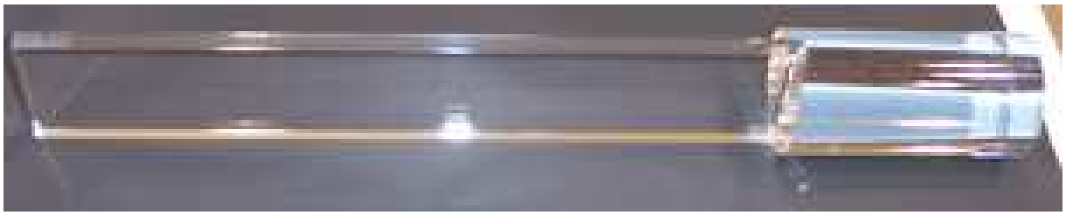

Figure 3: Lumi detector.

Figure 4: Lumi detector installation around the beam pipe.

Data were not taken with the Hall A HRS Spectrometers during this run. The beam energy was 5.019 GeV. BCM1 used for beam current measurements.

5 Electronics

The signals from the Lumi monitors were fed into the HAPPEX ADCs [5]. These are custom-built 16-bit integrating VME ADCs designed for high resolution and low differential non-linearity (DNL). For each helicity window, the ADC integrates the Lumi signal for 32 ms (starting 700 μs after the start of the window). Pseudorandom noise ('DAC noise') is injected into the integrated signal before digitization, and then removed in software to suppress DNL. Two different gain settings are available, and both settings were used at different times, in order to maintain the signal near the maximum of the ADC range. The standard HAPPEX parity-DAQ (which uses CODA) was used to generate timing and gate signals for the ADCs. The beam current and position from BCMs and BPMs in the hall were read out using the same ADCs.

Oversampling: The ADCs can operate in an 'oversampling' mode, in which they perform integration and digitization on a shorter sampling interval than the 32 ms default; some data were taken with oversampling factors of 3 ('OS=3') and 13 ('OS=13'). Unless otherwise stated explicitly, the data presented in this report were obtained with OS=3.

6 Data-taking and Analysis

For most of the data-taking, the Lumi gains (high voltages) and the ADC gain settings were adjusted between runs to maintain similar signal heights as seen at the ADCs. This was to ensure that electronic noise (*i.e.*, the pedestal width) was small compared to the data. Data from runs at different gains can't be directly compared for the luminosity (*i.e.* for the bulk effect), but the widths (fluctuations) should be independent of gain. This was confirmed using runs at the same beam current with different gain settings. Typically we maintained the ADC peaks somewhere between 20,000 and 55,000 counts, with pedestals around 4,000 counts, and pedestal widths about 12 counts. Typical runs were 5 minutes long.

In a second mode of data taking, for the luminosity scans, the beam was slowly ramped up to 100 μA, with the Lumi high voltages fixed. Here the widths are compromised at lower beam currents by electronic noise, and so they were not considered in the analysis. The relative luminosity was determined from the means of the pedestal-subtracted ADC peaks[1]. In addition, a few regular runs that had beam trips were also analyzed as luminosity scans; the normal ramping rate used by MCC was slow enough to get reasonable luminosity scan results.

The typical data used to study fluctuations are shown in Fig. 5. These plots show, for the thick carbon target (594 mg/cm^2), the "window-pair' asymmetry for the beam current (from BCM1 and BCM2) and for two of the Lumi detectors. These asymmetries are calculated from

$$\text{Asymmetry} = \frac{N^+ - N^-}{N^+ + N^-}$$

where N^+ and N^- represent the ADC values for two consecutive 33 ms time windows.

There was a non-zero beam current asymmetry for this particular run, which is seen in the mean values for both the BCMs and the Lumi detectors. What is relevant here, however, are the widths of the Lumi distributions; in the following, when Lumi widths (σs) are reported, they are just the σs of such

[1] As will be seen, when the target 'boiling' was bad, the peaks became decidedly non-Gaussian, so the mean of the ADC spectrum was used rather than the centroid of a Gaussian fit.

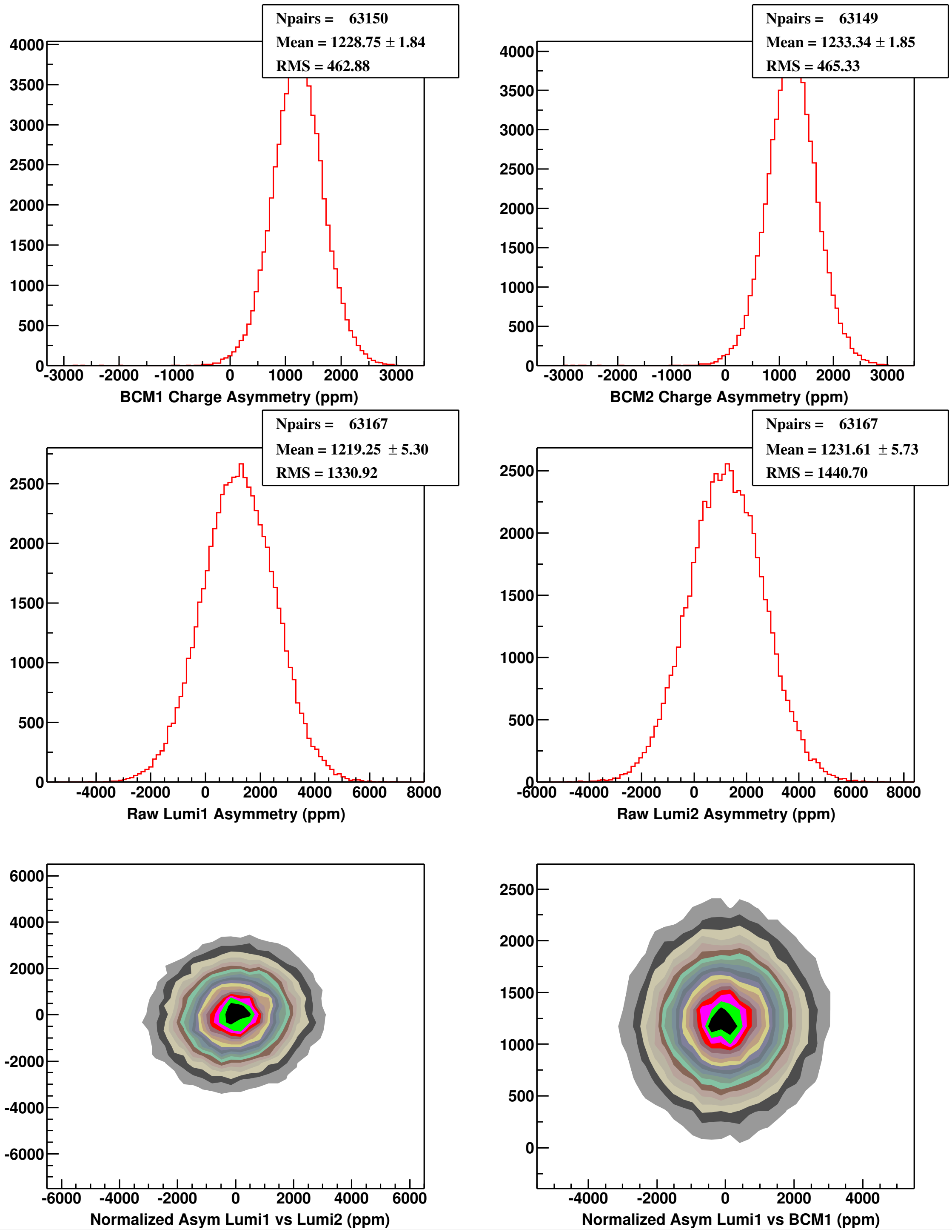

Figure 5: Typical Carbon target data. Window-pair asymmetry distributions for beam current (upper row), and for Lumi 1 and Lumi 2 (middle row) are shown. Normalizing the Lumi data to the BCM data on a pair-by-pair basis eliminates the effect of the non-zero beam current asymmetry (lower row), and one sees that the two Lumis provide statistically independent measurements.

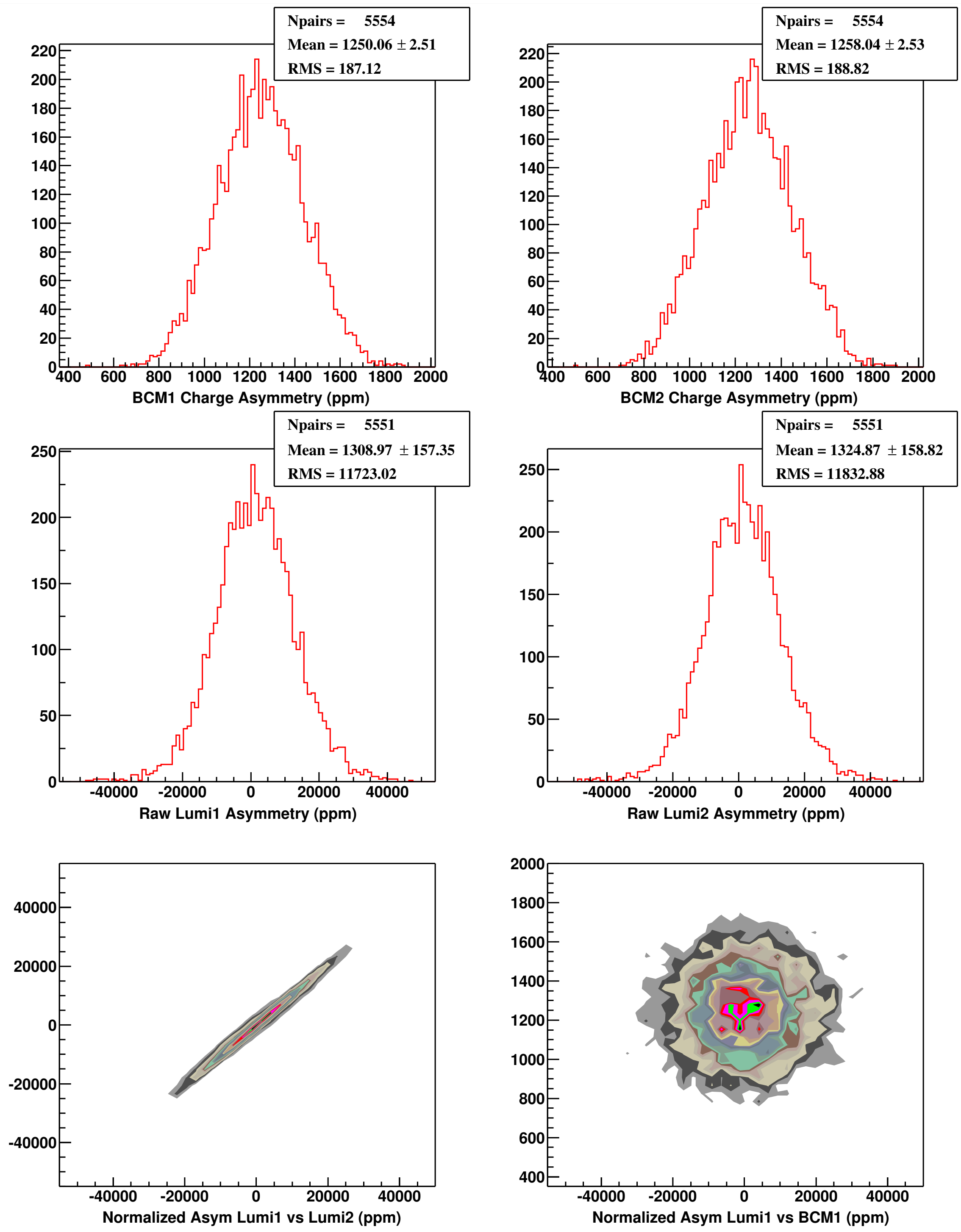

Figure 6: Typical lH_2 target data (15 cm cell). Window-pair asymmetry distributions for beam current (upper row), and for Lumi 1 and Lumi 2 (middle row) are shown. Here the data from the two Lumi detectors (after normalizing by beam current) are not statistically independent, due to target density fluctuations (lower left plot).

distributions.

Figure 6 shows typical asymmetry plots for the cryotarget. Note the much larger RMS widths for the Lumis than for carbon, and that, unlike the case for the carbon target, the two Lumi detector signals are highly correlated, indicating the presence of target density fluctuations. The width of the correlation stripe in the lower left plot of Fig 6 is a measure of the intrinsic counting-statistics widths of the Lumi distributions for these data.

The effect of beam motion on these data is small. One particular run (Run 2212) had (for an unknown reason) large ($\sim$ 2 mm) periodic excursions in horizontal beam position from the nominal values. The Lumi widths were seen to be essentially independent of beam position, and the ADC mean values change 2-3% per mm shift in beam position for Lumi 1 and Lumi 2, and 0.15% for Lumi 3 (which is located at a much larger scattering angle). Typical run-to-run variations in beam position were much smaller than this. The fact that all three detectors gave consistent results in all the results presented below indicates that any beam position effects are tiny, and so we did not attempt to correct for them.

A summary of all the runs taken, and the extracted Lumi detector amplitudes and widths is available at http://www.jlab.org/~suleiman/Boiling/runsummary.txt.

7 Results

Figures 7, 8, and 9 show the fluctuation results (asymmetry widths *vs.* beam current) measured for the 15 cm lD_2 target, with oversampling set to 13, 3 and 1 respectively, with a raster setting of 2.8 mm$\times$2.8 mm, and 60 Hz target fan speed, for various beam currents. Here, and elsewhere in this report, the statistical error bars on the widths are typically smaller than the data points, and are not shown.

In each case, one sees that the asymmetry width deviates from counting statistics (*i.e.*, from $\sigma \propto \frac{1}{\sqrt{I_{beam}}}$) somewhere between 20 and 40 μA, and rapidly blows up at higher beam currents, as target density fluctuations dominate the widths.

The trends are the same for all three Lumi's, with Lumi 3 showing larger σ's, consistent with a smaller counting rate, as expected. The different σ's found when measured with different oversamplings are consistent with the broadening expected from the reduced statistics of a smaller sampling window.

Figure 10 shows the fluctuation results for the 15 cm lH_2 target (2.8 mm$\times$2.8 mm raster, 60 Hz fan speed, OS=3). Again, the widths deviate from counting statistics somewhere below 20 and 40 μA. Compared to the deuterium target, the target fluctuations are roughly a factor of 2 larger at the same beam current (11,000 ppm *vs.* 5,500 ppm at 100 μA, with OS=3).

Figure 11 shows the fluctuation results for the 4 cm lH_2 target (2.8 mm$\times$2.8 mm raster, 60 Hz fan speed, OS=3). Again, the widths deviate from counting statistics somewhere below 20 and 40 μA. However, the increase in fluctuations is more gradual with beam current than with the 15 cm lH_2 and 15 cm lD_2 cells. It is not clear why this is the case.

To confirm that we really were at or very near counting statistics for low beam current, we took a couple of extra runs at 10 μA current with the 4 cm lH_2 cell, in which we increased the raster size to 3.8 mm$\times$3.8 mm, then in addition increased the target fan speed to 70 Hz. As discussed below, when fluctuations are large these two changes are observed to significantly reduce the fluctuations; at this beam current neither the fluctuations nor the bulk effect were affected (data not shown; the data agree within the size of the plotted points in Fig. 11), confirming that we were at counting statistics under these conditions.

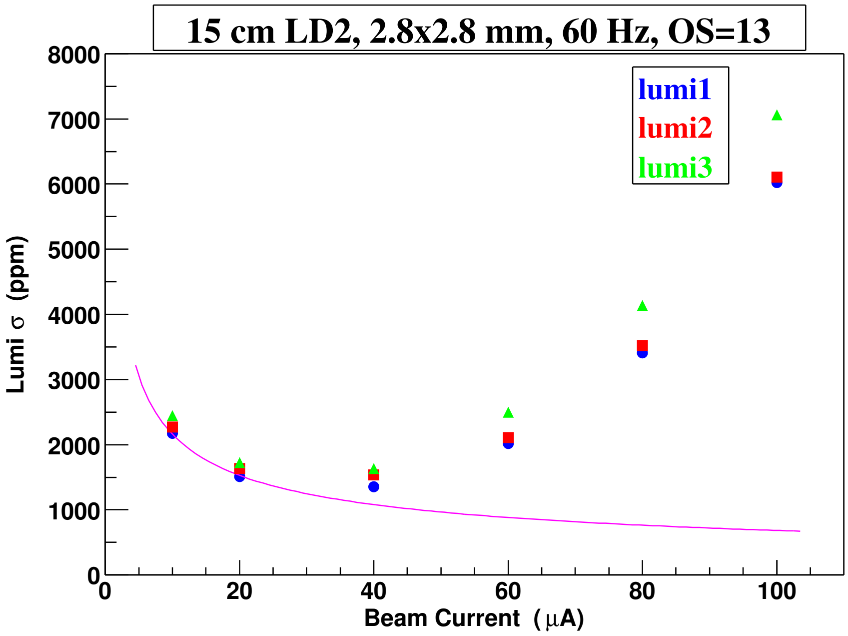

Figure 7: 15 cm lD_2 (OS=13) Lumi Sigma *vs.* Beam Current. Counting statistics dependence shown by line.

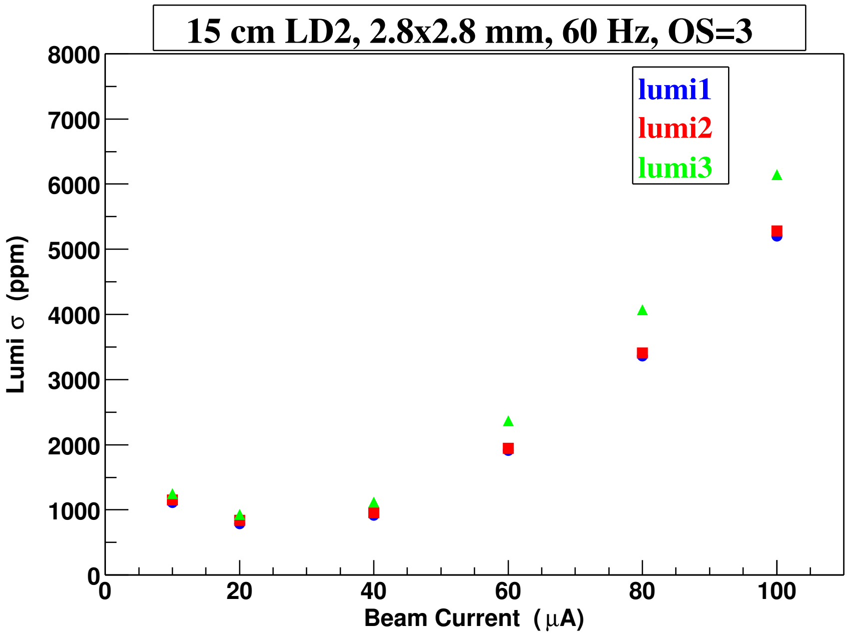

Figure 8: 15 cm lD_2 (OS=3) Lumi Sigma *vs.* Beam Current.

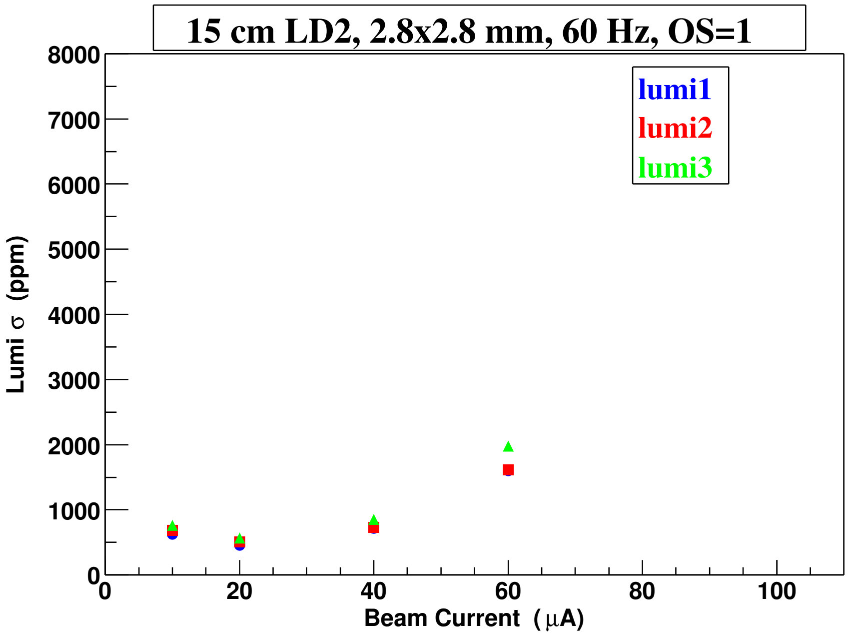

Figure 9: 15 cm lD_2 (OS=1) Lumi Sigma *vs.* Beam Current.

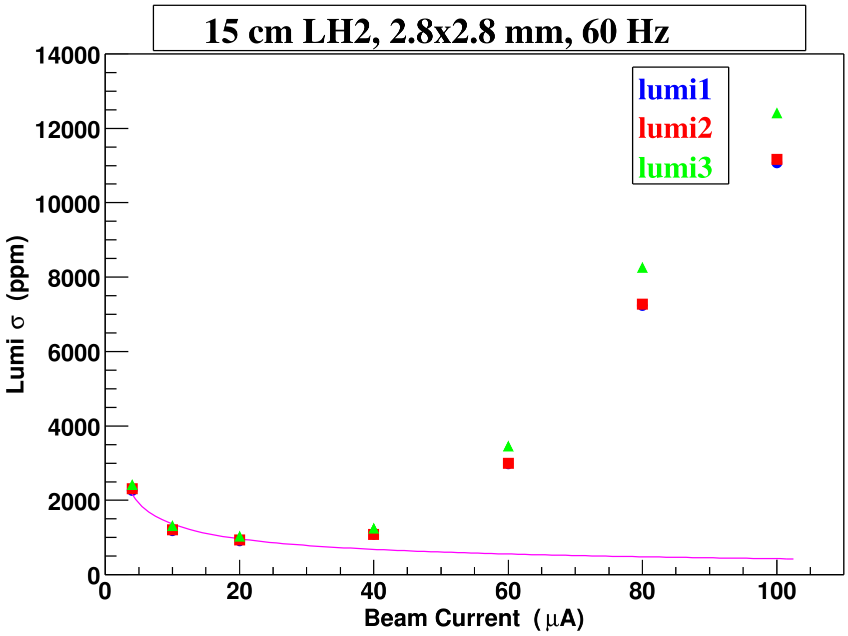

Figure 10: 15 cm lH_2 (OS=3) Lumi Sigma *vs.* Beam Current. Counting statistics dependence shown by line.

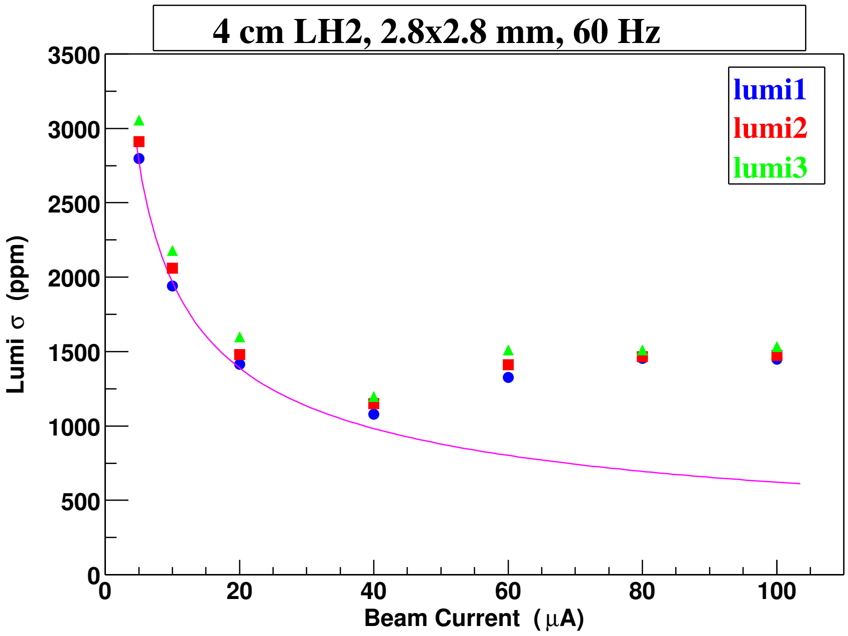

Figure 11: 4 cm lH_2 (OS=3) Lumi Sigma *vs.* Beam Current. Counting statistics dependence shown by line.

Figures 13 and 12 show the fluctuation results for the thick carbon target, for two different over-sampling rates. Here, the data follow pure counting statistics at all beam currents as expected (*carbon doesn't boil!*). Note that the statistical widths imply that the rate that the Lumi detector was seeing was of order 250 MHz at 100 μA.

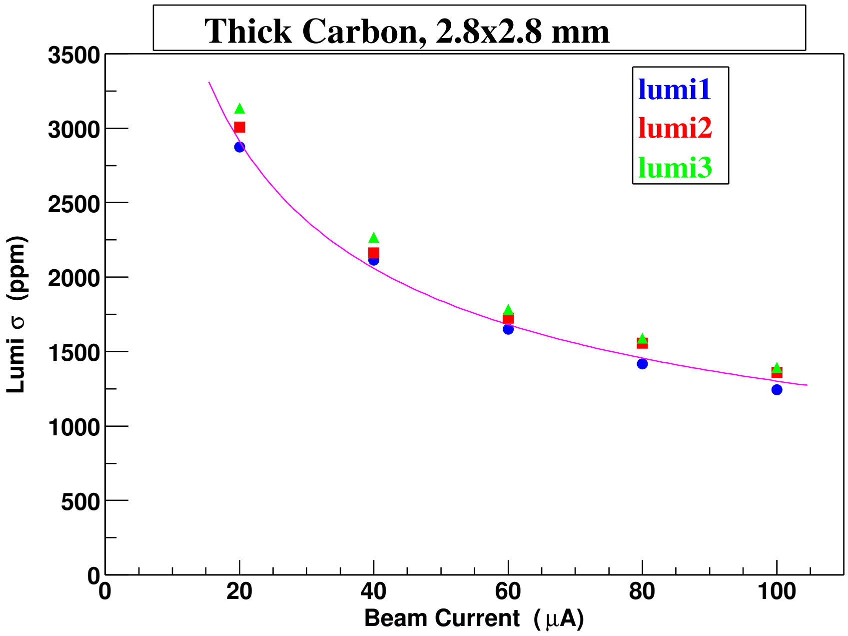

Figure 12: Carbon target (OS=13) Lumi Sigma *vs.* Beam Current. Counting statistics dependence shown by line.

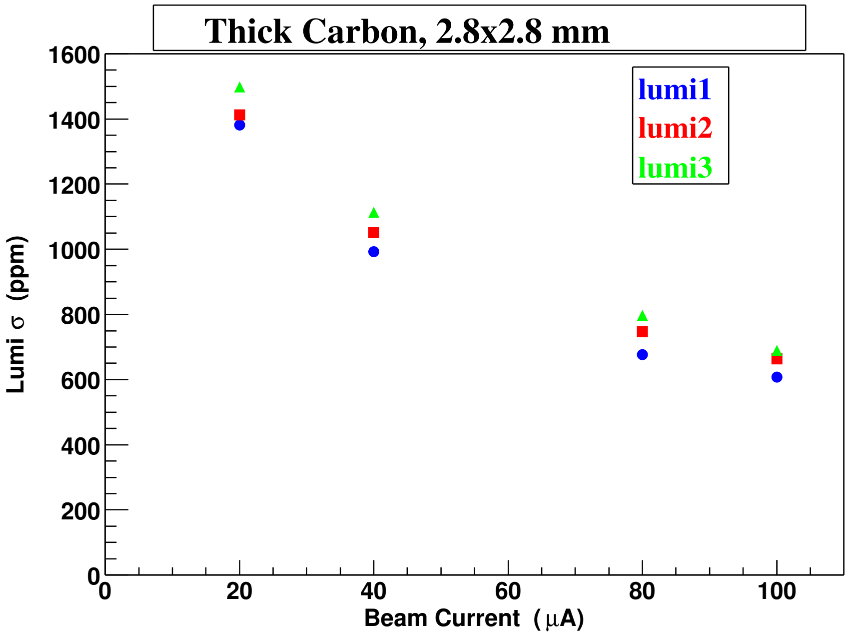

Figure 13: Carbon target (OS=3) Lumi Sigma *vs.* Beam Current.

Figure 14 shows the mean ADC value *vs.* beam current (the 'bulk effect') for various configurations. These data were either from deliberate beam ramps or from beam trips (in which case the data are noisier). The decrease in target luminosity is seen clearly for the 15 cm lH_2 and lD_2 cells, and as expected the slopes increase as the raster size is decreased. In all cases, the bulk effect appears to vary roughly linearly with beam current; there is no clear evidence of a 'threshold' beam current where the effect 'turns on'.

As expected, there is no significant effect for the carbon target (the small increase seen thus provides a measure of our systematic error). The 4 cm lH_2 shows little or no bulk effect (with the 2.8 mm$\times$2.8 mm raster, 60 Hz fan speed), despite the fact that under these conditions the fluctuations at 100 μA were already significant (twice counting statistics, see Fig. 11). Thus the fluctuations can become important under conditions where the bulk effect is still rather small ($< 1\%$) and hard to measure: 15 Hz fluctuations are a more sensitive indicator of target density effects than the bulk luminosity change.

The slopes are given in Table 1. The small positive slope seen for the carbon target probably indicates effects due to beam halo variation when the beam was ramped; we thus estimate that the precision on our measured slopes is no better than $\pm 4\%$. The slopes found here are consistent with typical values found in previous studies with cryotargets at JLab; see Appendix A.

Target	Raster (mm $\times$ mm)	Fan Speed (Hz)	Slope $(100\ \mu A)^{-1}$
Carbon	2.8×2.8	-	3.6 %
lD_2 (15 cm)	1.4×1.4	60	-10 %
lH_2 (15 cm)	1.4×1.4	60	-21 %
lH_2 (15 cm)	2.8×2.8	60	-5.3 %
lH_2 (15 cm)	3.8×3.8	60	-2.3 %
lH_2 (4 cm)	2.8×2.8	60	0.2 %

Table 1: Bulk effect slopes: % change in apparent luminosity for a beam current change from 20 μA to 100 μA, based on Lumi 1.

A clear dependence of the slope on the raster size is seen. The slope is much smaller for the 4 cm lH_2 cell than for the 15 cm lH_2 cell. The slope for lD_2 is about half that for lH_2 under the same conditions; this is consistent with trends from previous results (see Appendix A).

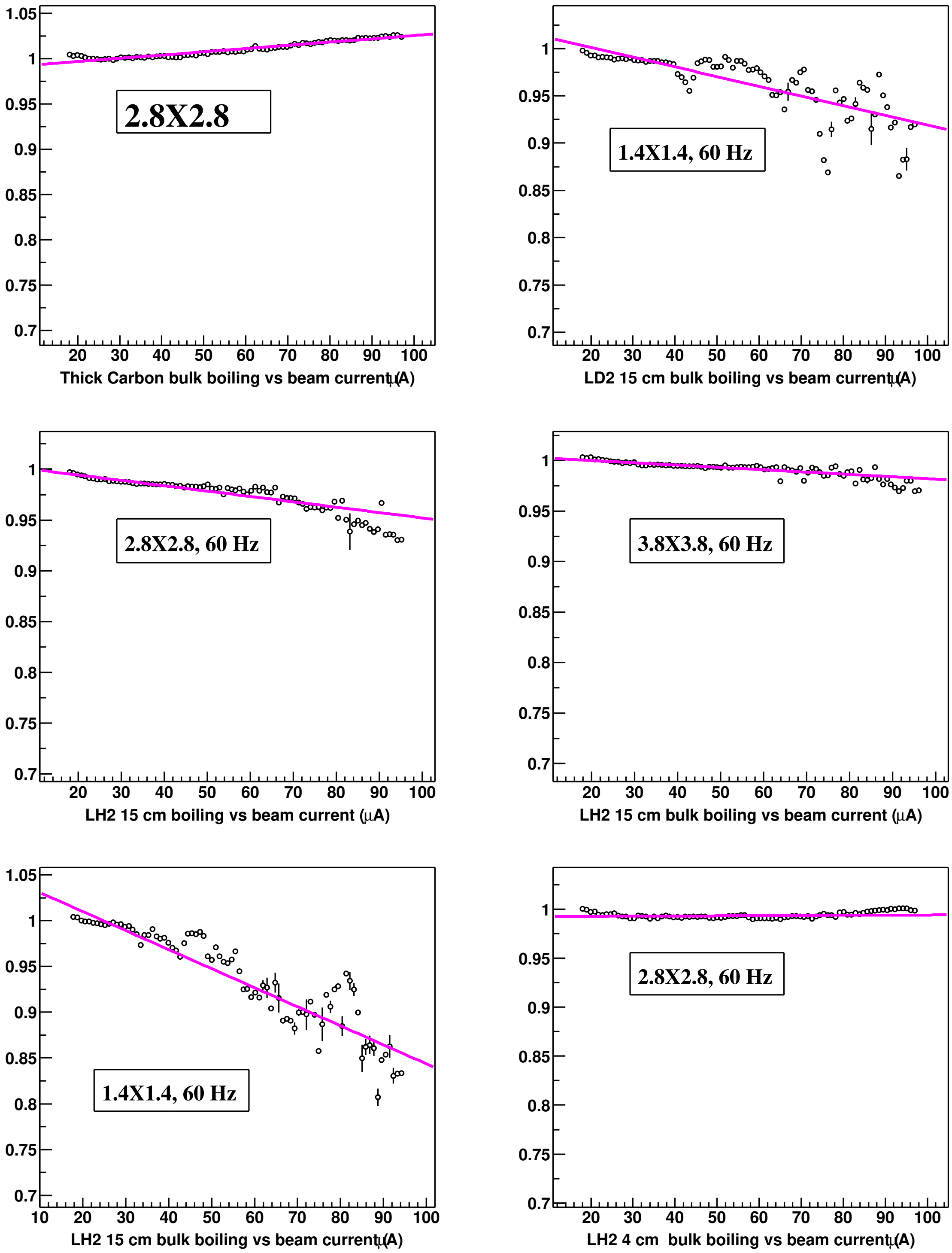

Figure 14: Bulk effect: relative ADC peak values (Lumi 1, normalized to beam current) *vs.* Beam Current for various configurations. Simple linear fits are shown, normalized to 1 at 20 μA. Data shown are for Lumi 1. The raster settings and fan speeds are indicated.

7.1 Target Fan speed

The effect of varying the target fan speed (and hence the fluid flow rate) is shown in Figs. 15, 16, (for 15 cm lH_2) 17, 18 (for 4 cm lH_2) 19, and 20 (for 15 cm lD_2). All data are taken at 100 μA beam current and with the same raster setting. Smooth decreases in the fluctuations and increases in the bulk effect luminosity (*i.e.*, the ratio of mean Lumi ADC to beam current) are seen as the fan speed is increased. In the bulk effect plots, the difference in the lumi/BCM1 values between different Lumi detectors at a given setting (*e.g.*, Fig. 16) just reflects differences in solid angles subtended and high voltage settings, and so is not of significance.

Note the 4 cm lH_2 results, which clearly show that the fluctuations blow up when the fan speed is decreased below 70 Hz, and yet the corresponding bulk effect is hardly changed: again, 15 Hz fluctuations are a very sensitive indicator of density changes in the target. Even at 70 Hz fan speed, counting statistics (about 750 ppm) is not achieved for this cell at 100 μA.

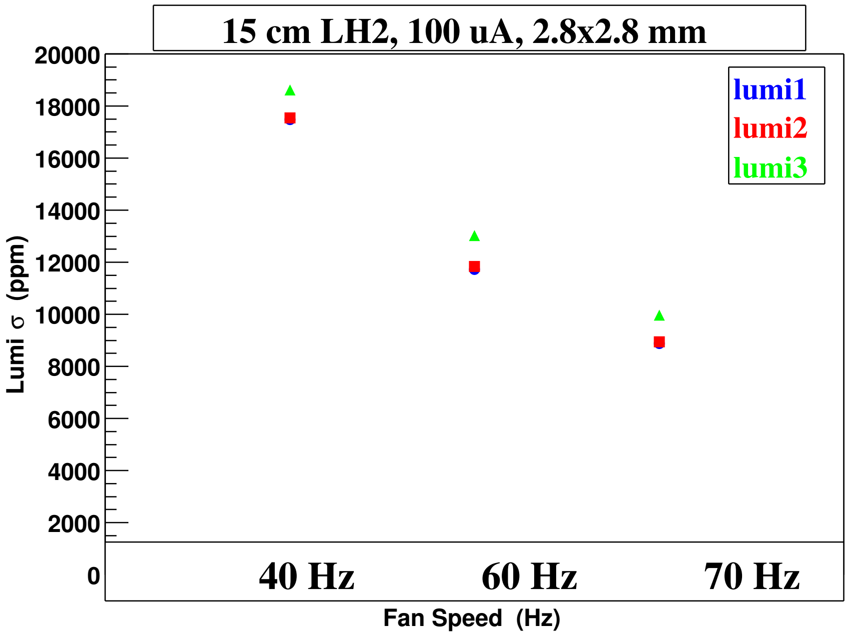

Figure 15: 15 cm lH_2 Lumi Sigma *vs.* Fan Speed.

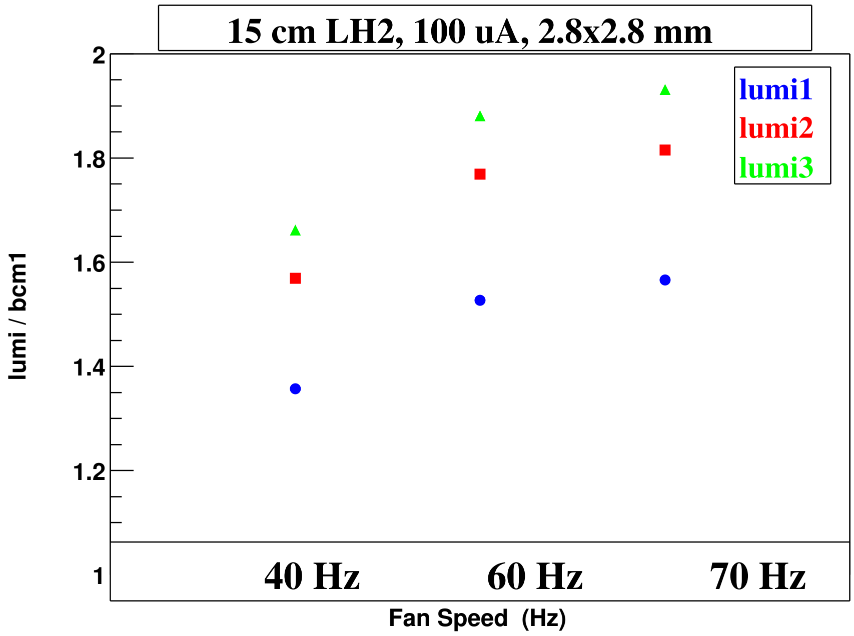

Figure 16: 15 cm lH_2 Lumi Bulk Effect *vs.* Fan Speed.

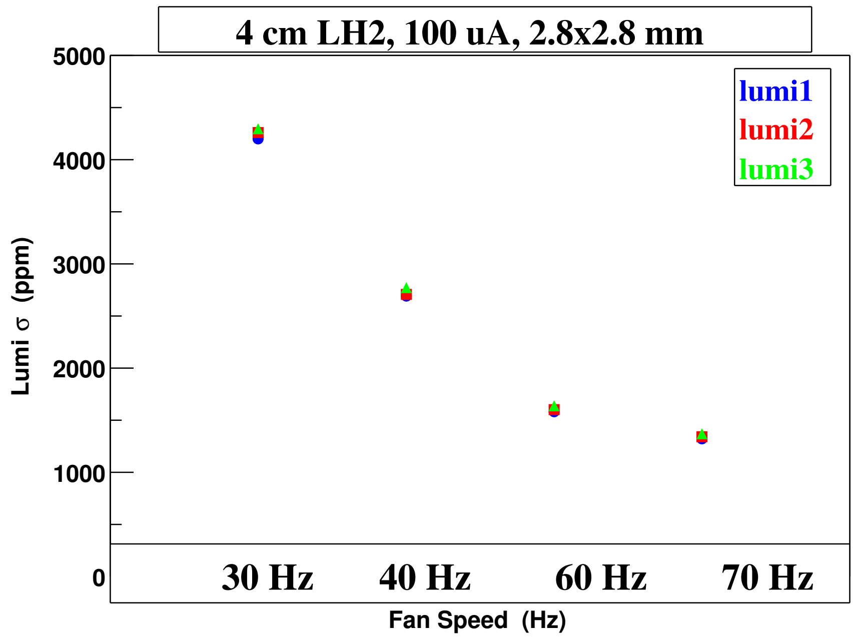

Figure 17: 4 cm lH_2 Lumi Sigma *vs.* Fan Speed.

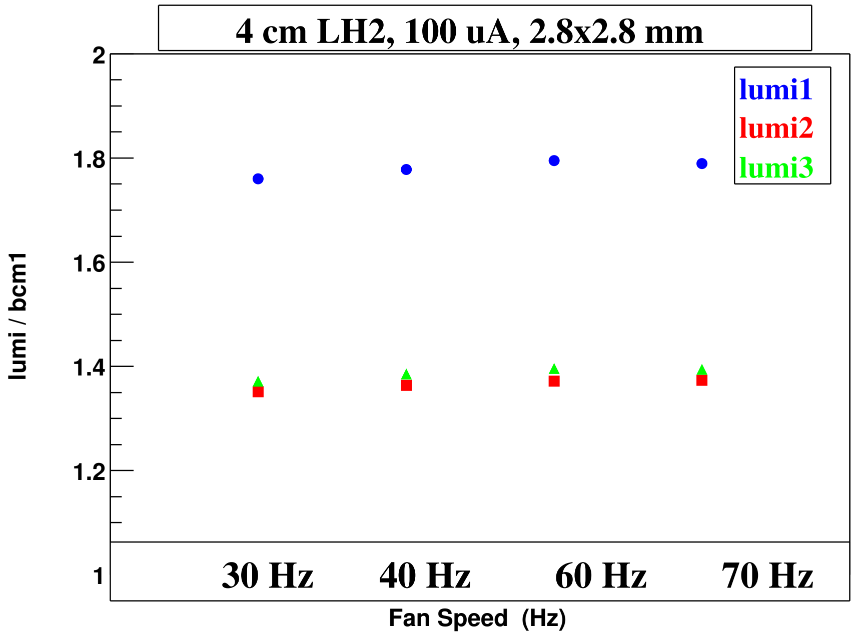

Figure 18: 4 cm lH_2 Lumi Bulk Effect *vs.* Fan Speed.

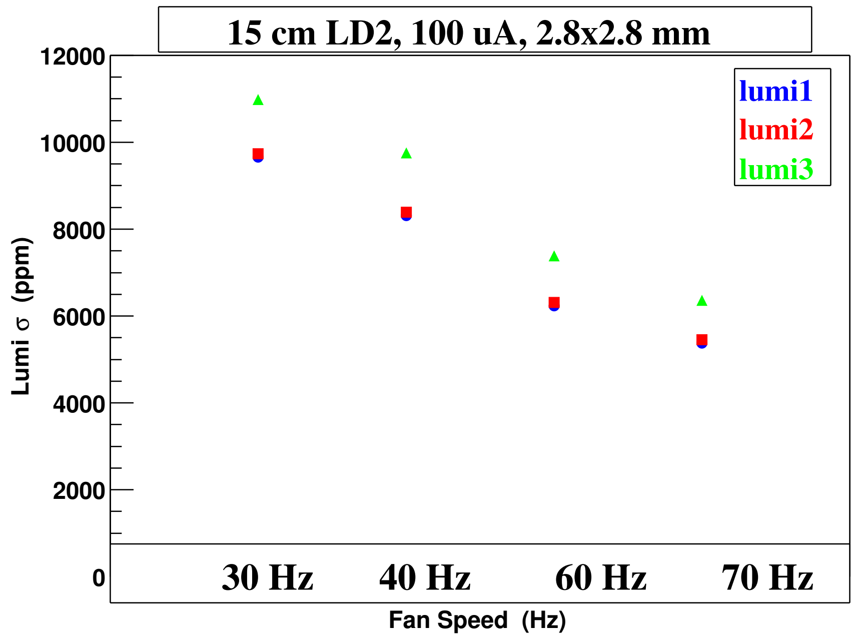

Figure 19: 15 cm lD_2 Lumi Sigma *vs.* Fan Speed.

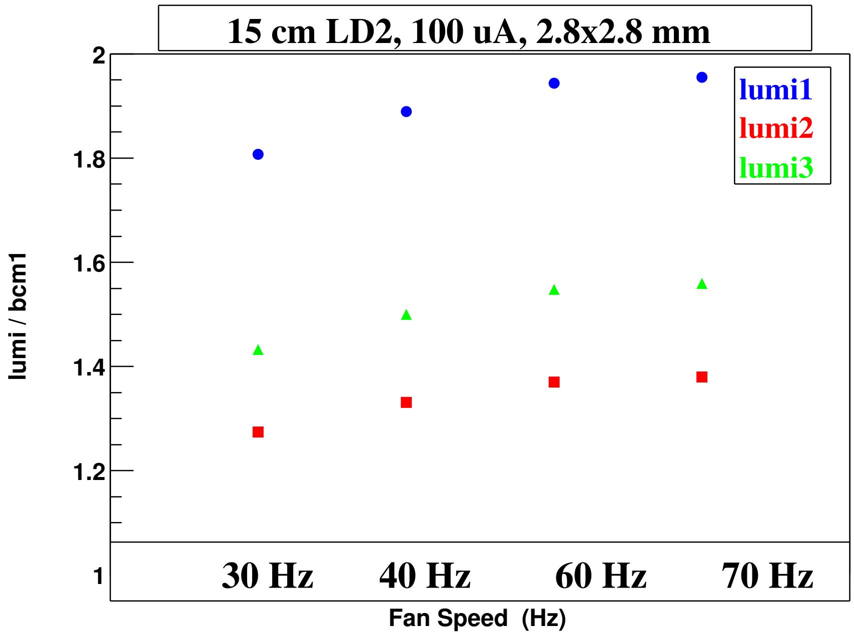

Figure 20: 15 cm lD_2 Lumi Bulk Effect *vs.* Fan Speed.

7.2 Raster Setting

Figures 21 and 22 show the fluctuations and bulk effect for the carbon target at 100 μA for various raster sizes; there is no change, as expected, thus confirming that the effects of the raster size on the cryotargets presented below are not artifacts of solid angle changes.

Figures 23, 24, 25 show the raster's effect on 100 μA data with the 15 cm lH_2 cell. Increasing the raster size decreases the fluctuations and increases the bulk luminosity.

Along with the three square raster settings, rectangular rasters in two different orientations (1.4 mm$\times$3.8 mm and 3.8 mm$\times$1.4 mm) were tested; the results were almost identical, indicating that rastering the beam along or perpendicular to the nominal (vertical) flow direction makes almost no difference - this is consistent with what one expects for highly turbulent flow. From Fig. 24 it seems that the fluctuations scale smoothly with the raster area.

Similar results are seen for the 4 cm lH_2 cell (see Figs 26, 27, 28) and the 15 cm lD_2 cell (see Figs. 29, 30, 31).

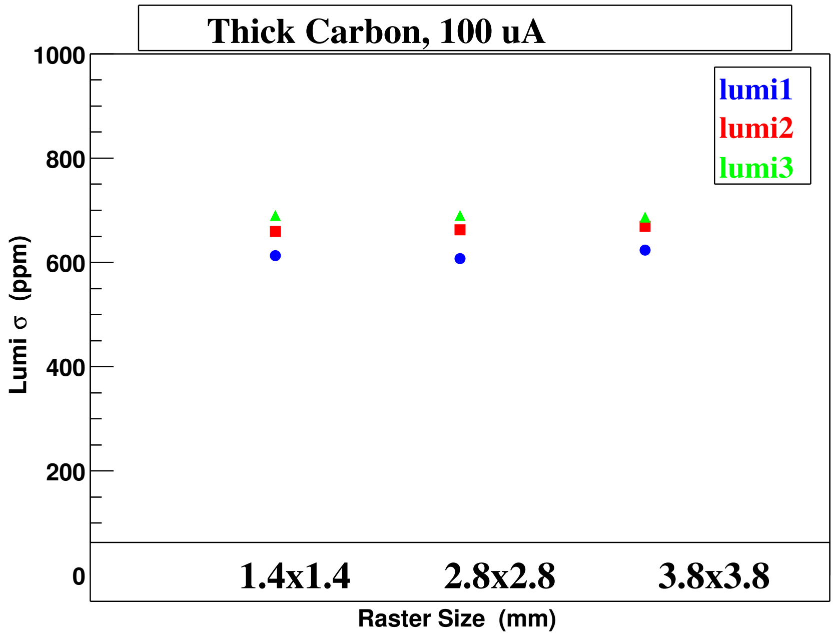

Figure 21: Carbon target Lumi Sigma *vs.* Raster Size.

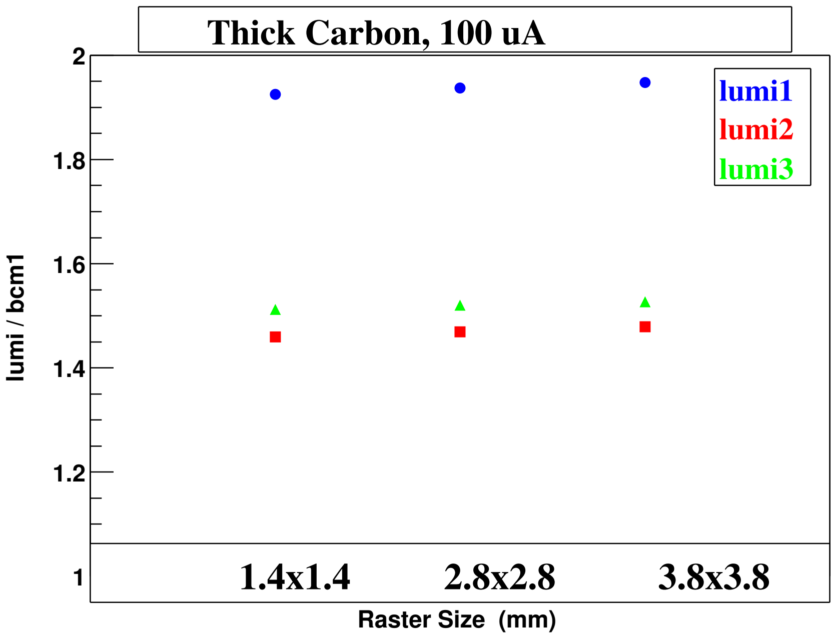

Figure 22: Carbon target Lumi Bulk Effect *vs.* Raster Size.

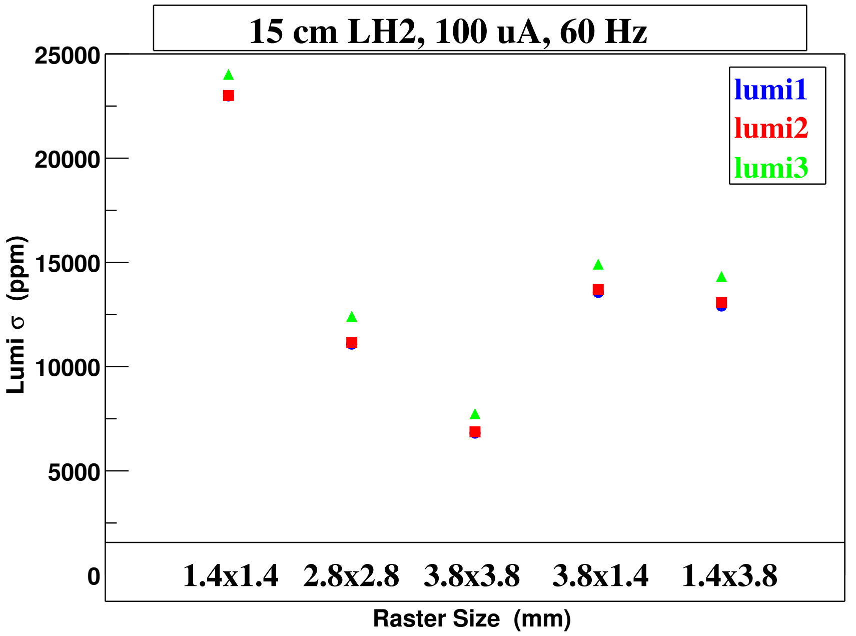

Figure 23: 15 cm lH_2 Lumi Sigma *vs.* Raster Size.

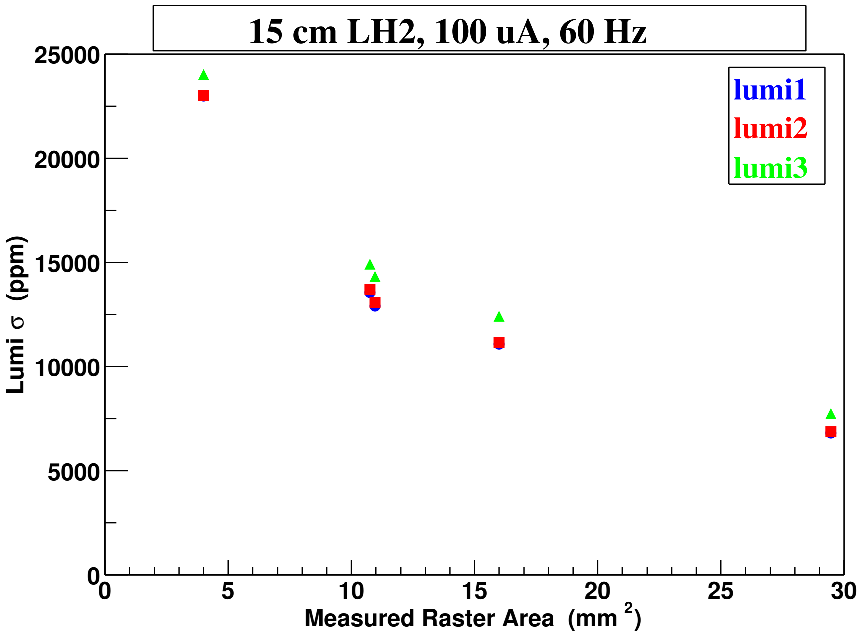

Figure 24: 15 cm lH_2 Lumi Sigma *vs.* measured Raster Area.

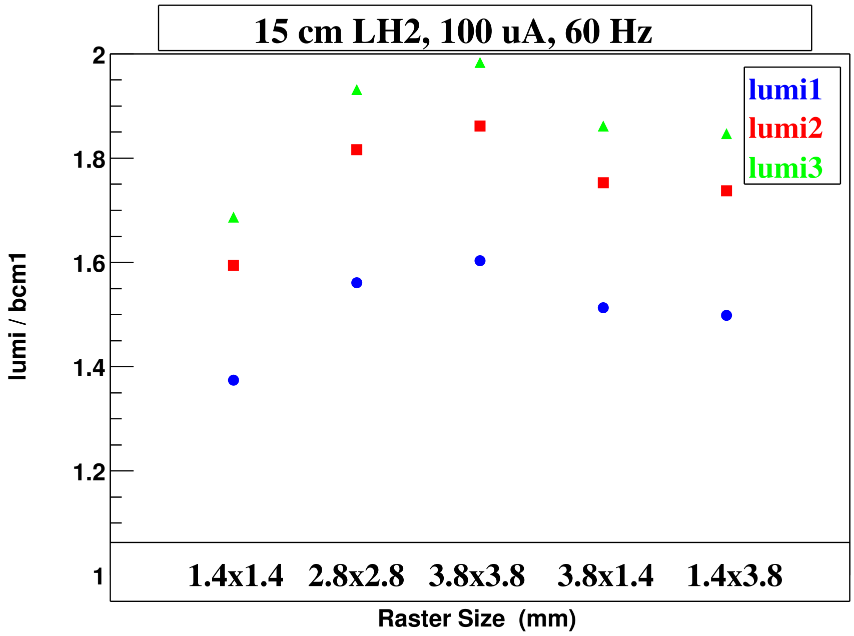

Figure 25: 15 cm lH_2 Lumi Bulk Effect *vs.* Raster Size.

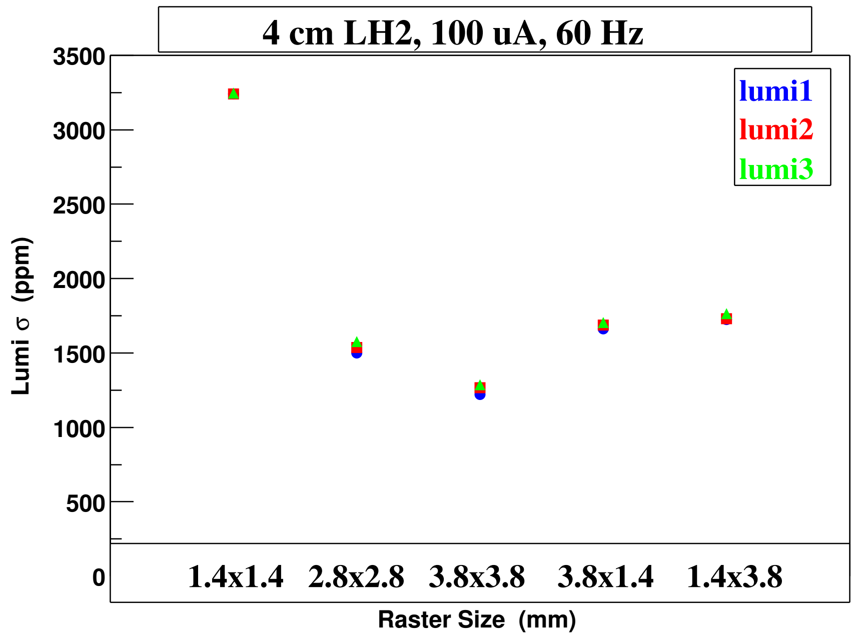

Figure 26: 4 cm lH_2 Lumi Sigma *vs.* Raster Size.

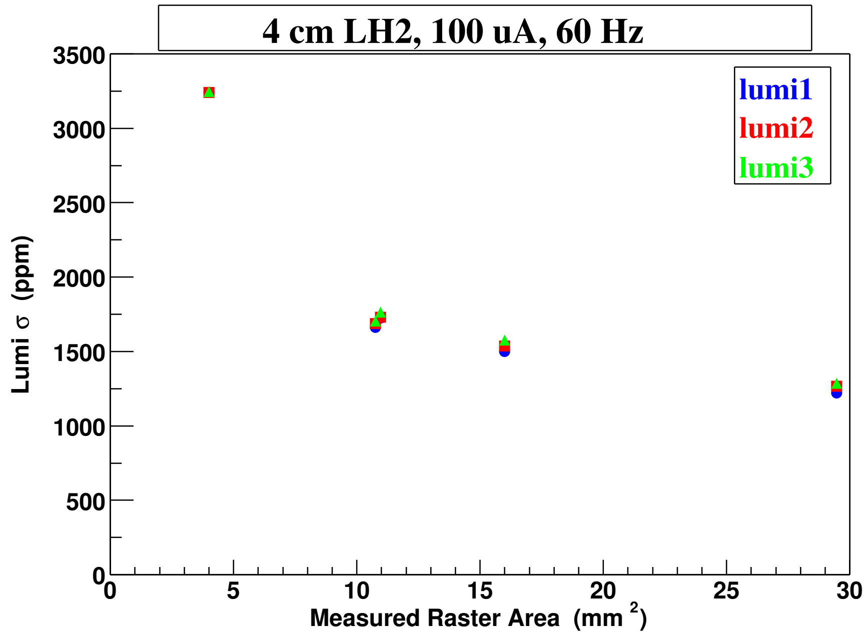

Figure 27: 4 cm lH_2 Lumi Sigma *vs.* Measured Raster Area.

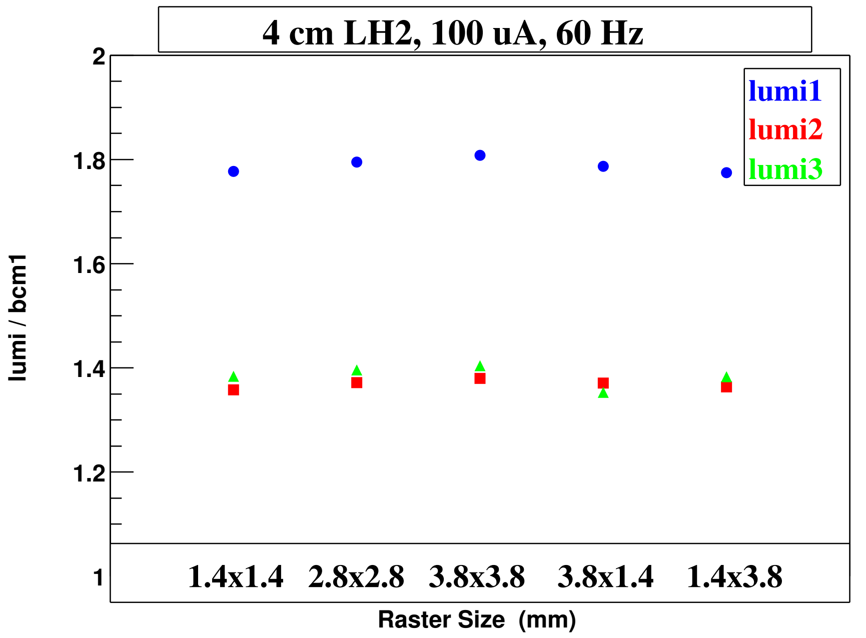

Figure 28: 4 cm lH_2 Lumi Bulk Effect *vs.* Raster Size.

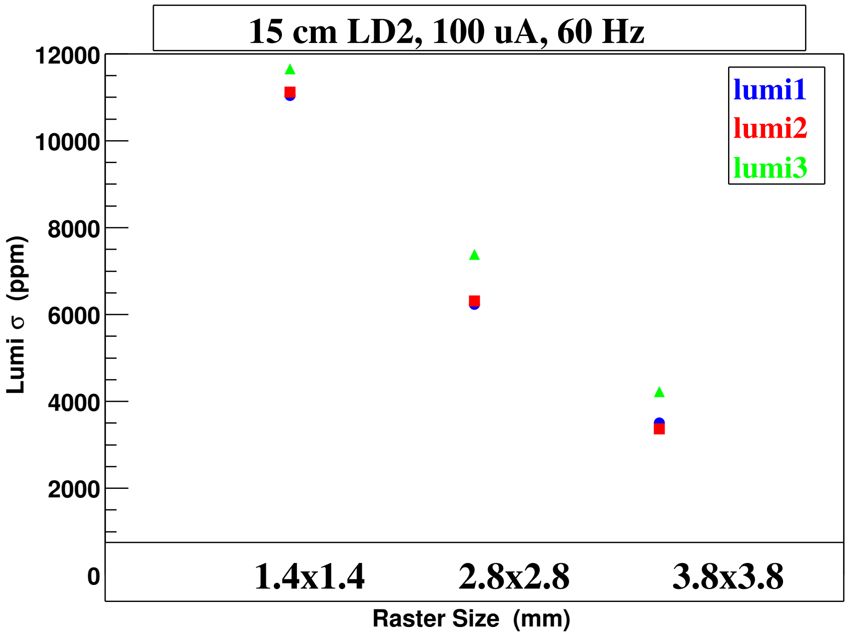

Figure 29: 15 cm lD_2 Lumi Sigma *vs.* Raster Size.

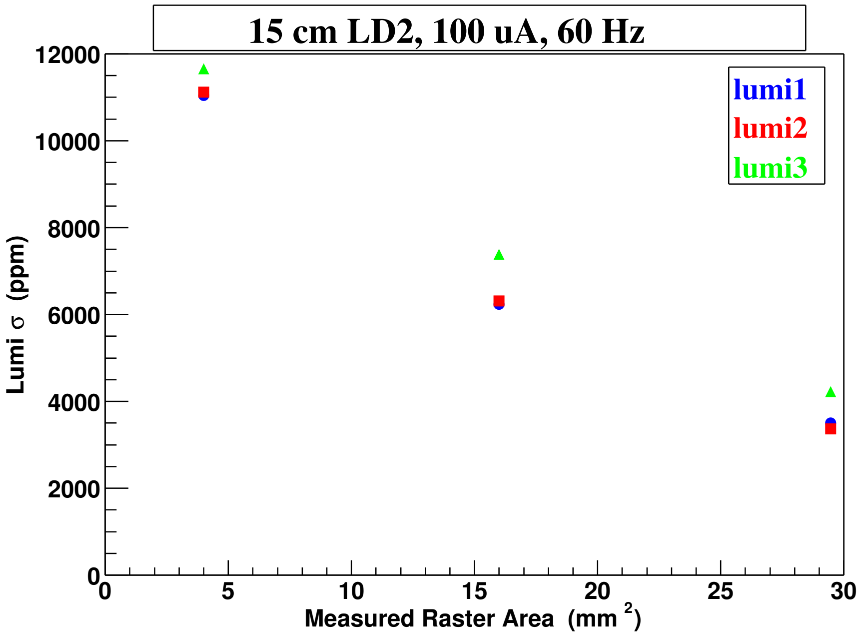

Figure 30: 15 cm lD_2 Lumi Sigma *vs.* Measured Raster Area.

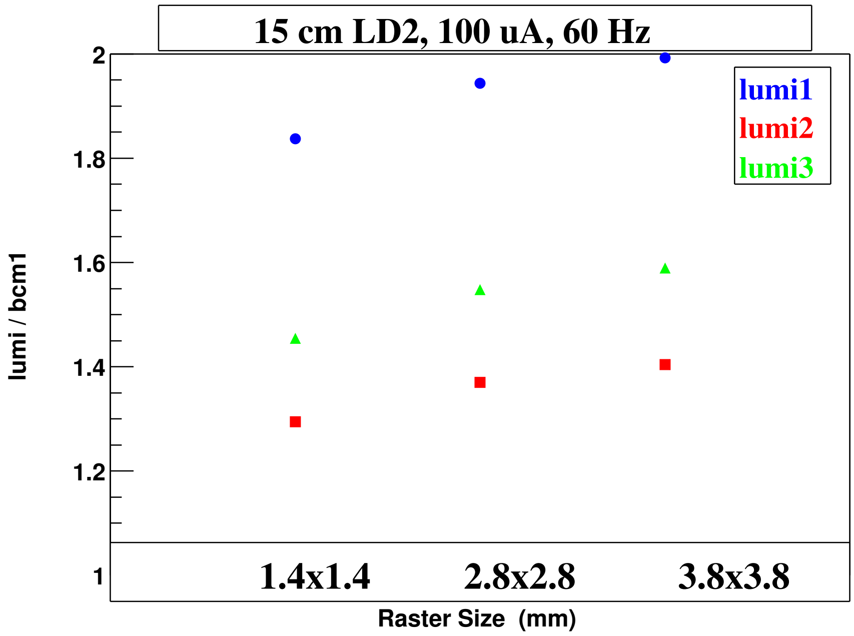

Figure 31: 15 cm lD_2 Lumi Bulk Effect *vs.* Raster Size.

7.3 Intrinsic Beam Spot Size

To test whether the intrinsic beam spot size has an effect on 'boiling' effects, we asked MCC to detune quadrupoles to increase the beam spot. The data discussed above were all taken with a spot of about 60 μm (x) by 150 μm (y), as measured at BPMs 4a and 4b, using harp scans with the raster off. The operators were able to detune to produce a spot of 190 μm (x) by 475 μm (y) measured in the same way. Note that this represents an increase in area of a factor of 10. All data with this 'huge' spot were taken with 100 μA beam, and OS=3.

Figure 32 shows the fluctuation results for the 15 cm lH_2 target *vs.* raster for both normal spot (closed markers) and the huge spot (open circles). The results with the 4 cm lH_2 target are shown in Fig. 33.

One clearly sees a decrease in the fluctuations with the increased spot size. With the 15 cm lH_2, the σ's decreased by 15-17% with the bigger spot; unfolding the σ's in quadrature, this is consistent with an effect of 6000 ppm (for the 2.8 mm$\times$2.8 mm raster) and 13,000 ppm (for the 1.4 mm$\times$1.4 mm raster). For the 4 cm cell, the effect is a reduction of 30%, 7%, or 3% (for the 1.4 mm$\times$1.4 mm raster, 2.8 mm$\times$2.8 mm raster, and 3.8 mm$\times$3.8 mm raster respectively), or, unfolding in quadrature, an effect of 2260 ppm, 540 ppm, or 250 ppm, respectively. Thus the effect of changing the beam spot size is largest when the 'boiling' is worst, and it has essentially no effect when the target density effects are already small, as might be expected.

Contrast these changes (for an order of magnitude change in the spot size) with the much larger effects seen for more modest relative changes in the raster area; see Figs. 32 and 33. Clearly the raster is much more important than the intrinsic spot size; one gains very slowly by blowing up the beam spot.

The bulk effect data for these runs showed effects of under a few %, and were not terribly consistent for the three Lumi monitors.

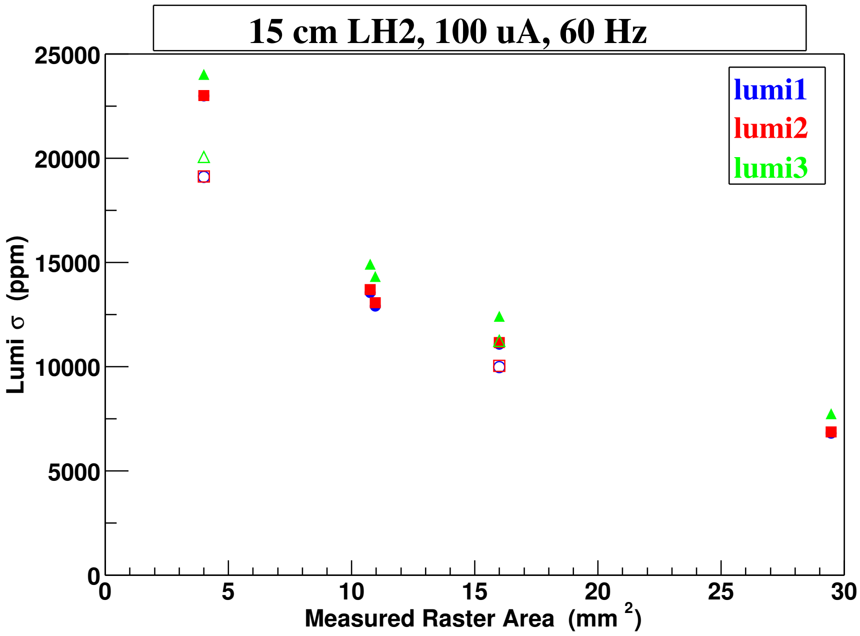

Figure 32: 15 cm lH_2 Lumi Sigma *vs.* Measured Raster Area, open markers larger spot size.

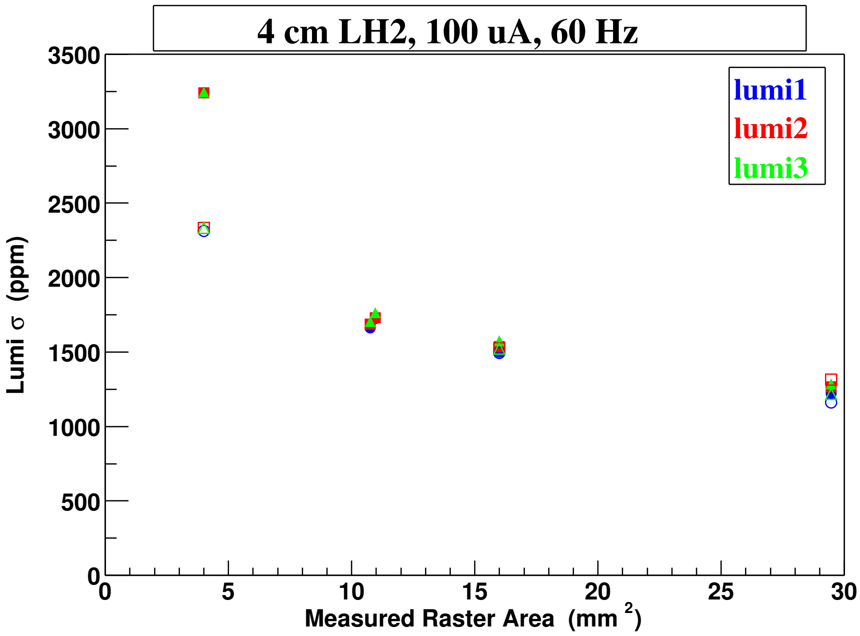

Figure 33: 4 cm lH_2 Lumi Sigma *vs.* Measured Raster Area, open markers larger spot size.

7.4 Fluctuation Time Scale

The characteristic time scale of the fluctuations can be determined from the oversampling data. Figure 34 shows the signal from one Lumi, normalized to beam current *vs.* time. Data with OS=13 are used (*i.e.*, measurements are made with 2.5 ms time bins). The carbon target result appears purely statistical, as expected, but the lD_2 target at 100 μA clearly shows the time-dependence of the target density; structure with time scales on the order of 100 ms is evident. Figures 35 and 36 show similar plots for lD_2 at different beam currents and different raster settings. The fluctuations disappear at 10 μA, consistent with our interpretation of the beam current dependence (recall Fig. 7).

Similar features are seen with the reduced oversampling setting (OS=3), although the effect is less clear since the bins get closer in size to the scale of the fluctuations. Similar results are seen with the lH_2 target.

Figure 37 shows that the observed fluctuations are identical as observed in two independent Lumi detectors - the effect is real.

Note that the observed fluctuation time scale (100 ms) is long compared to the raster frequency (20 kHz); the entire rastered spot is 'painted" by the beam 50 times in the time between two data points in these plots. Note also that the expected flow speed of the fluid ($\sim$ 60 cm/s) through the beam spot is fast on this time scale; the entire volume of fluid in the rastered spot should be replaced in 5 ms for a 3 mm-wide raster. This might argue either that the fluctuations are dominated by a fluctuating "static" bubble at the target window, or that the flow velocity locally in the cell is much less in some region (the far end?) of the cell.

The relatively slow time scale of these fluctuations is also consistent with the earlier observation that the intrinsic beam spot size is less important than the raster area; on the time scale of the fluctuations, the beam 'seen" by the target is the rastered size.

If one is not successful at reducing the fluctuations by changing target/beam properties, there are two other possible solutions for a parity experiment:

1. Change to a much higher helicity flip rate. The smoothness of the data on a bin-to-bin basis in the lower plot of Fig. 34 suggests that on the scale of 2.5 ms the effect of fluctuations is reduced by an order of magnitude. Thus running at $\geq$ 400 Hz would help.

2. Normalize the asymmetry pairs using the luminosity monitor instead of the beam current. However, the lumi monitor response is much more sensitive to beam position effects than the BCMs, and so this would entail attendant new problems.

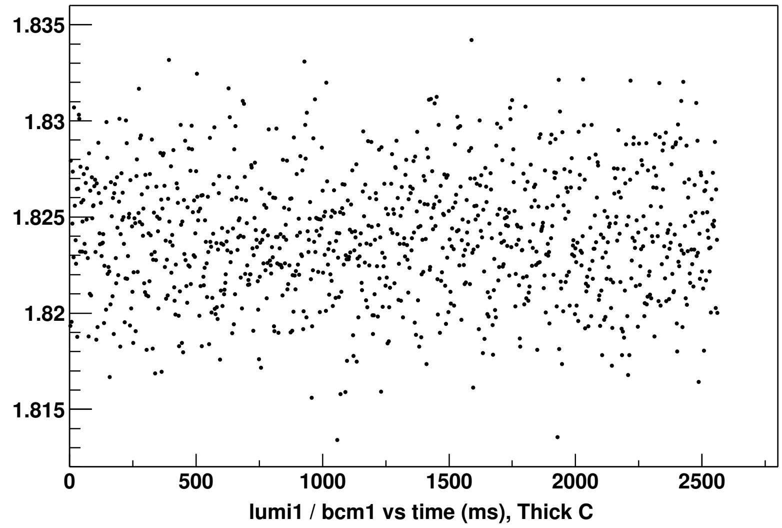

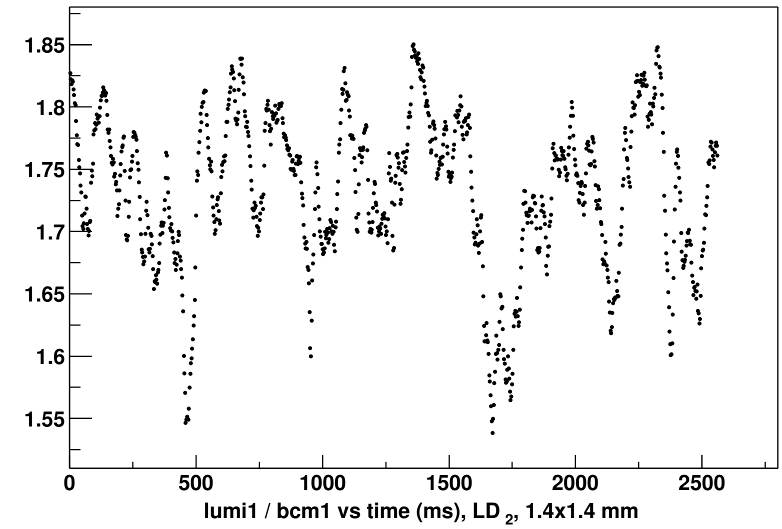

Figure 34: Lumi 1 signal, normalized by beam current, *vs.* time, for 100 μA, OS=13, carbon target (upper plot) and 15 cm lD_2 (lower plot). The characteristic fluctuation time scale for the lD_2 is clearly seen to be of order 100 ms.

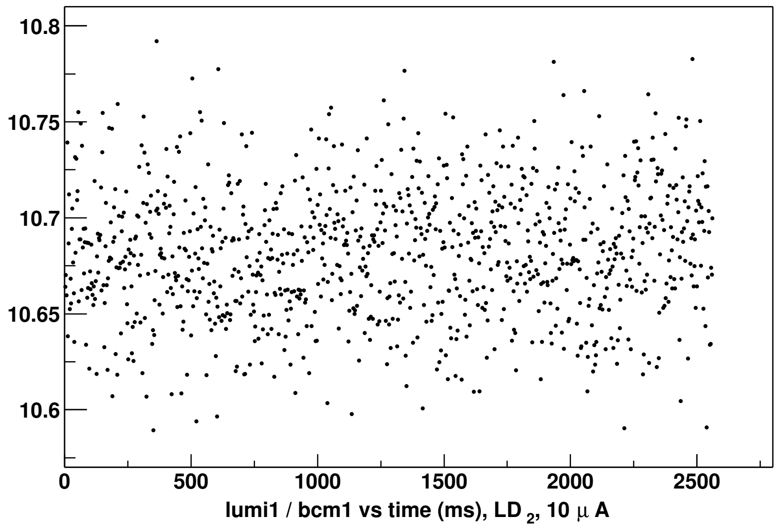

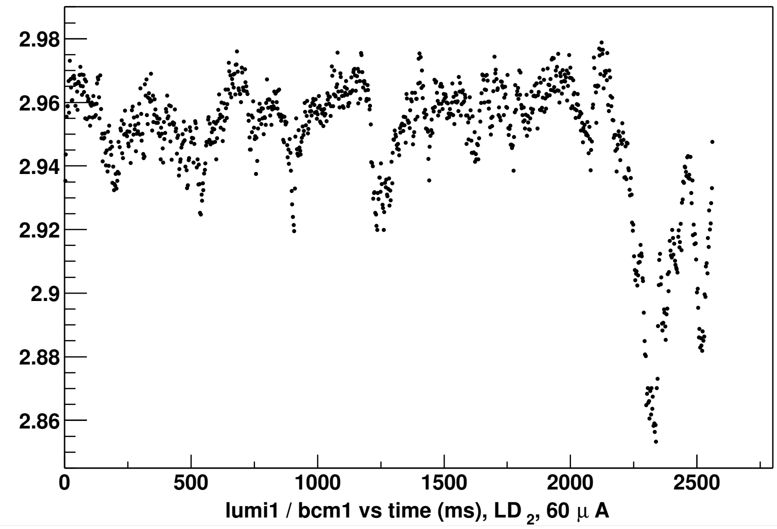

Figure 35: Lumi 1 signal , normalized by beam current, *vs.* time, for 15 cm lD_2, OS=13, at 10 μA (upper plot) and 60 μA (lower plot). The fluctuations are gone at low beam current.

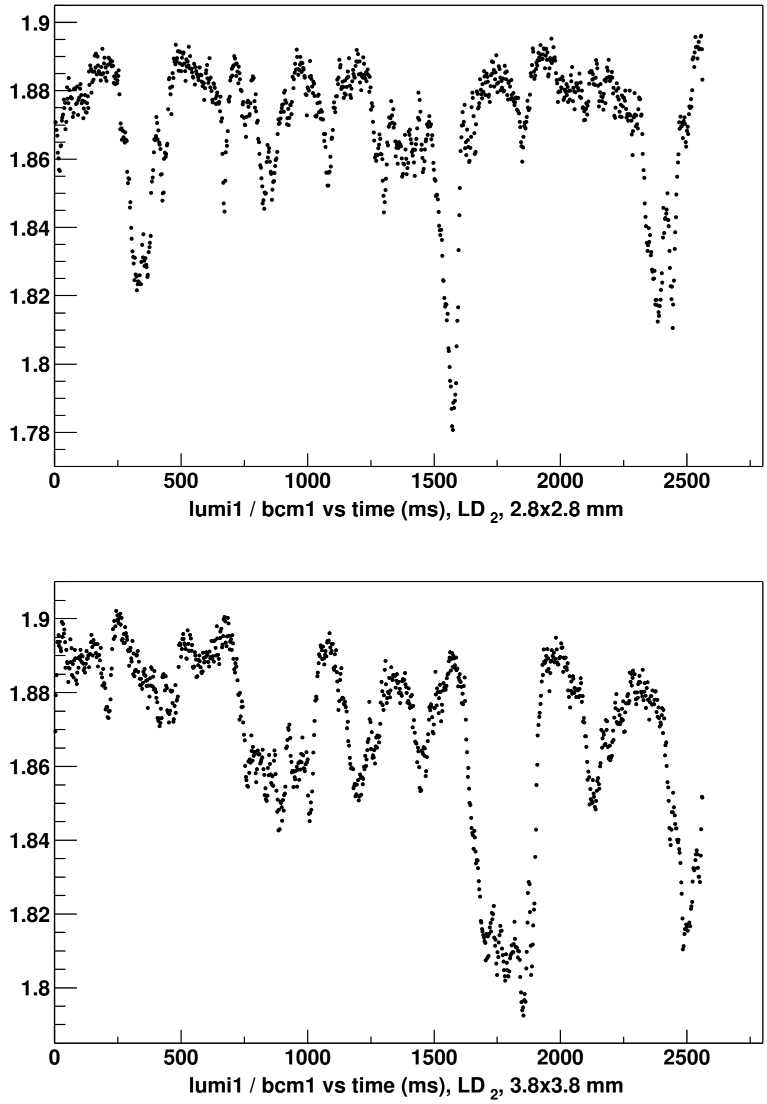

Figure 36: Lumi 1 signal , normalized by beam current, *vs.* time, for 15 cm lD_2, OS=13, at 100 μA, with 2.8 mm×2.8 mm raster (upper plot) and 3.8 mm×3.8 mm raster (lower plot).

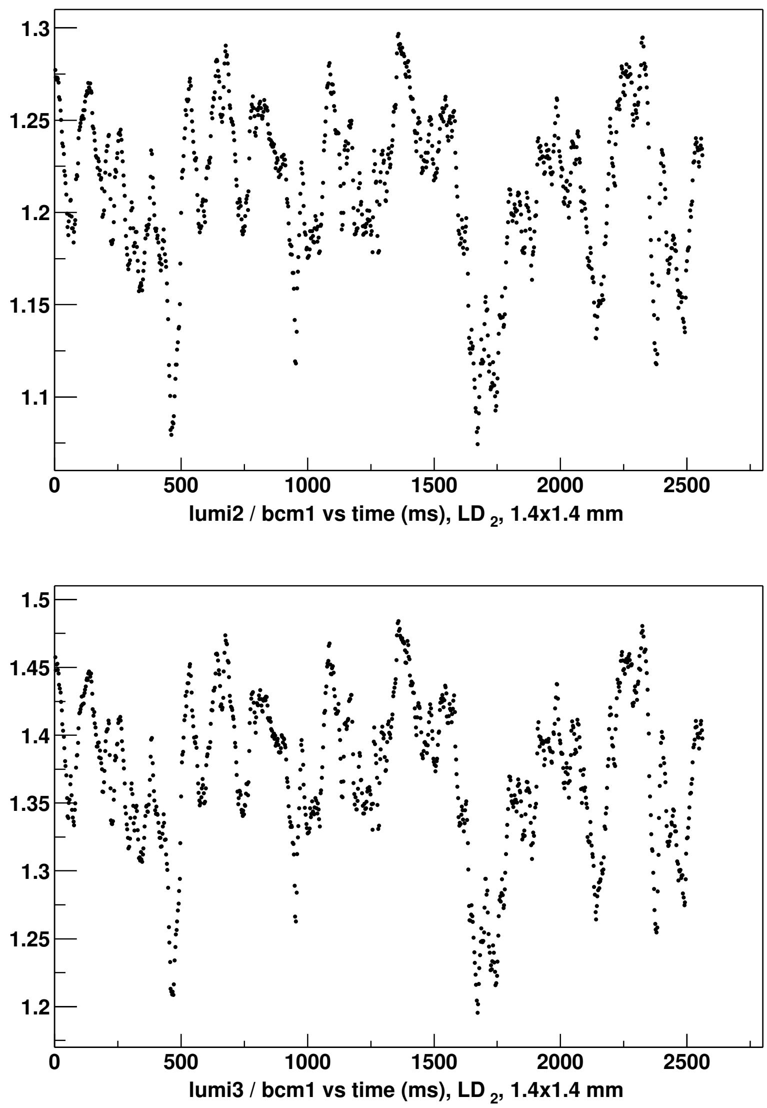

Figure 37: Lumi 2 signal (upper plot) and Lumi 3 signal (lower plot), normalized by beam current, *vs.* time, for 15 cm lD_2, OS=13, at 100 μA. Independent detectors see the same density fluctuations.

7.5 Scaling of Fluctuations with Bulk Effect

Generally speaking, for a given target, the fluctuations scale smoothly with the bulk effect loss in luminosity. Figure 38 shows the relation between the fluctuations (σ's) and the relative Luminosity (mean ADC values, 3 Lumi's averaged, normalized to beam current) for a number of runs taken with different targets, beam currents, raster settings, and fan speeds. The relative luminosity was determined by extrapolating to zero beam current. Not all the data taken at different beam currents is shown, only those results obtained with the same high voltages on the Lumis is included.

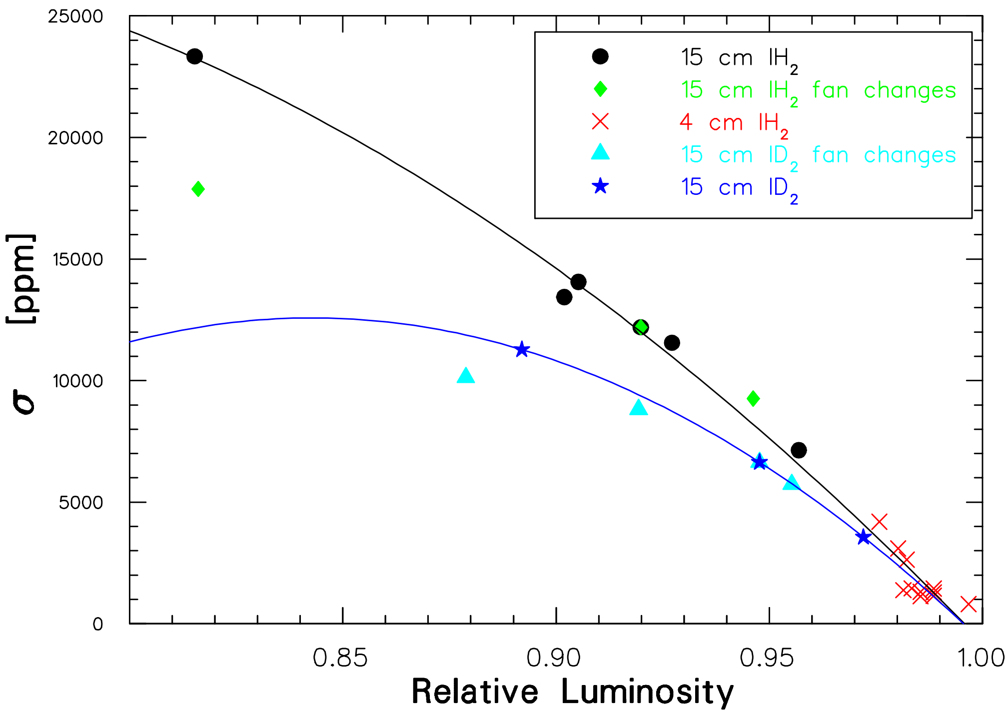

Figure 38: Fluctuation widths *vs.* Relative Luminosity, for various targets, raster and fan settings, and beam currents; all data with same high voltages and ADC gain setting, OS=3. The lines represent quadratic fits to the lH_2 (black) and lD_2 (blue) data respectively. For both Relative Luminosity and the σ's, results are averages of the three 3 Lumi detectors.

One sees that, except perhaps when the boiling is very high, all the data from both the 15 cm and 4 cm lH_2 cells lie approximately on the same curve; the lD_2 data lie on a distinctly different curve: for the same bulk density loss, the fluctuations (at 30 Hz) are less for lD_2 than for lH_2. This may be a useful clue as to the mechanism leading to the fluctuations.

There is also some evidence that changes in the target fan speed (as opposed to beam current or raster changes) lead to a somewhat different relation between σ and the bulk effect (see the green diamonds and cyan triangles in Fig. 38). Increasing the fan speed (fluid flow) seems to decrease the fluctuations proportionally more. This would suggest that differences in fluid flow are more critical than beam power density in reducing the fluctuations.

One should compare the data in Fig. 38 with that obtained in the HAPPEX-I experiment. With target/raster/beam conditions that were measured (using the HRSs) to give a bulk effect of 0.95 (5% loss

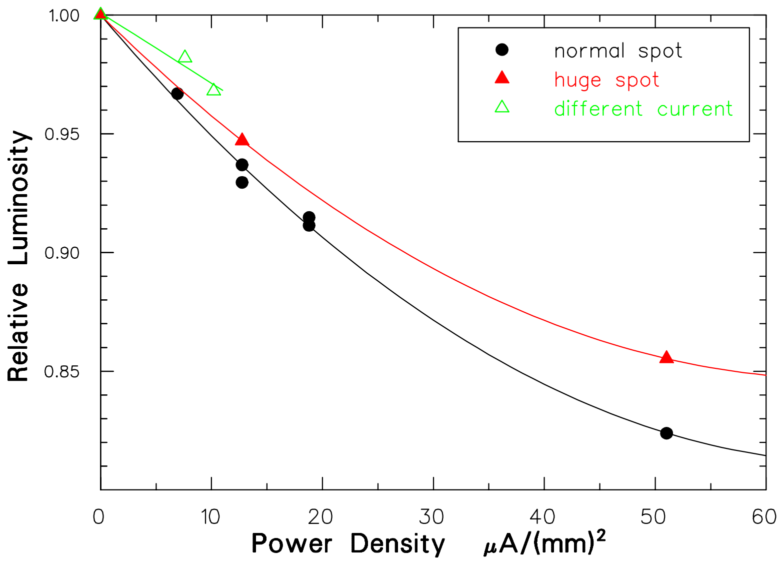

Figure 39: Relative Luminosity *vs.* Beam Power Density, for the 15 cm lH_2 cell, 60 Hz fan speed, OS=3. The black circles are data taken at 100 μA, for various raster settings, with the normal beam spot, the red closed triangles are similar data taken with the 'huge' intrinsic beam spot, and the green open triangles are data taken with the normal spot, but at lower beam currents. The fits are simple quadratic or linear fits, forced to go through relative Luminosity = 1 at zero power density.

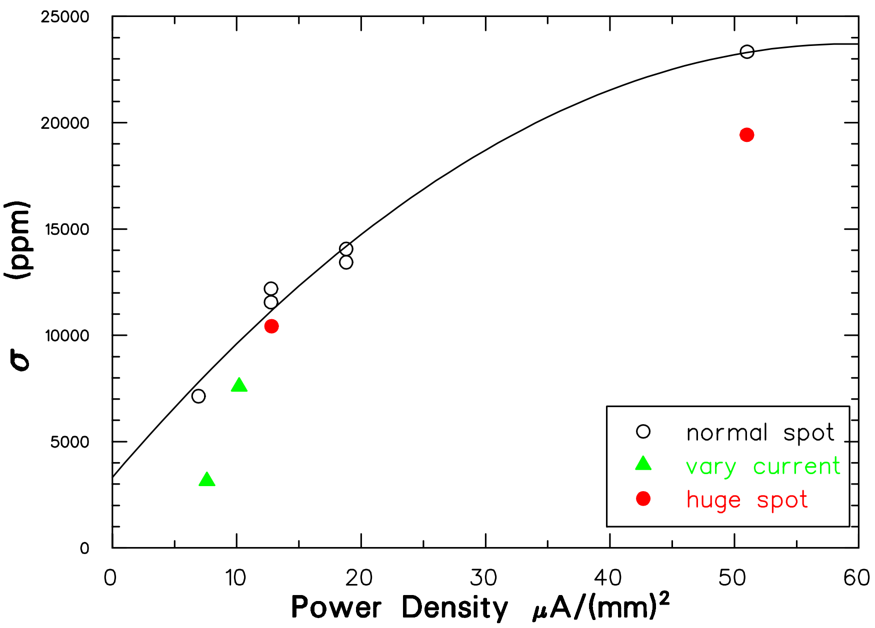

Figure 40: Fluctuations vs. Beam Power Density, for 15 cm lH_2 cell, with normal beam spot at 100 μA, various raster sizes (open circles), various beam currents (closed green circles) with constant raster size, and with 'huge' beam spot (closed red circles).

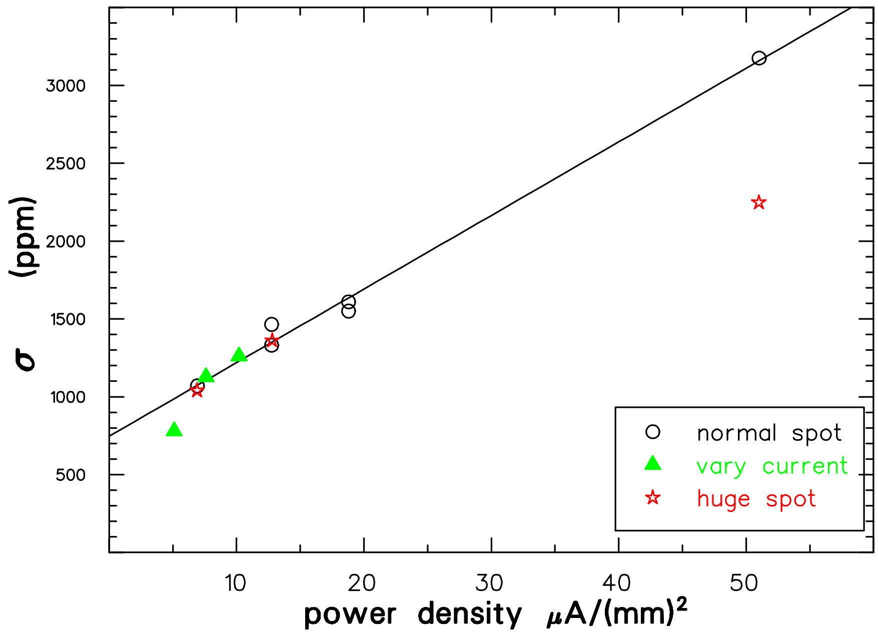

Figure 41: Fluctuations vs. Beam Power Density, for 4 cm lH_2 cell, with normal beam spot at 100 μA, various raster sizes (open circles), various beam currents (closed green circles) with constant raster size, and with 'huge' beam spot (closed red circles).

in apparent cross section), the fluctuations in lH_2 were measured to be of order 250 ppm; *this is more than an order of magnitude smaller than what is seen in Fig. 38 (order 7,500 ppm at 0.95).*

As the raster, fan speed, beam current conditions were similar between the present data and the HAPPEX-I data, and as the intrinsic beam spot effect has been shown to be small, the only remaining aspect that can explain the reduced fluctuations in HAPPEX-I is the cell geometry[2]. The cells used for HAPPEX-I were 15 cm long, 6.5 cm diameter 'beer can' cells. Perhaps the larger diameter (6.5 cm *vs.* 3.65 cm for the present cells), the exit window thickness (3.5 mil *vs.* 5 mil), or perhaps the shape of the exit window (flat with rounded edges *vs.* spherical section) causes the difference. Unfortunately, we did not have 'beer can' cells available to test in our study.

A simple expectation might be that the fluctuations and/or the bulk effect should scale just with the beam power density, *i.e.,* with beam current over raster area [3]. Figure 39 shows the bulk effect as a function of the power density, for the 15 cm lH_2 cell. The dependence appears quadratic, but the curves are different for different intrinsic beam spot sizes. The data taken at one beam current, but varying the raster area (black open circles), do not lie on the same curve as the data taken by varying the beam current, keeping the raster area fixed (open green triangles). Thus the simple expectation is clearly too naive. This is also seen in Fig. 40 in which it is seen that the fluctuations do not simply scale with the power density. In order to minimize the fluctuations one does better by reducing the beam current than

[2]It is true that the bulk effect data were taken during a different running period than the fluctuation data for HAPPEX-I; however the bulk effect data were taken twice, in Oct. and Dec. 1997, with reproduceable results, and with results in accord with other data; the direct measurement of boiling fluctuations for HAPPEX was done in Oct 1997, in a special low-Q^2 run, however, the main data-taking runs over several months in Spring 1998, Spring 1999 and Summer 1999, showed no evidence for increased asymmetry widths due to target boiling.

[3]Note that the area used in the power density calculation is the area of the raster setting; the raster area at the target being a factor of $(1.4)^2$ larger, these power densities should really be divided by a factor of 2.

increasing the raster area, at a constant power density. Similar behaviour is seen with the 4 cm LH_2 cell; see Fig. 41.

8 Sanity Checks

- The fact that the fluctuations depend in a smooth and sensible manner on both target fan speed and the raster area clearly indicates that the fluctuations are due to the physics of the target, not spurious properties of the Lumi detectors or the analysis method.
- Similarly, the fact that the carbon target shows fluctuations that scale with beam current as expected for pure counting statistics, and shows no significant bulk effect also reinforces the fact that the effects with the cryotargets are real properties of the target. The carbon target data were also obtained with three different raster settings, with no resulting changes in the widths: thus the raster effect seen with the cryotarget is real, and not a solid-angle effect.
- With the carbon target, the data taken with different values of oversampling at a given beam current had widths that just scaled with the counting statistics as expected for the different sampling windows (*e.g.* $\sqrt{13/3}$ for OS=3 *vs.* OS=13), again confirming counting statistics for system when the cryotarget is not used.
- At low beam currents (5 and 10 μA) with the 4 cm lH_2 target, the widths (and amplitudes) were independent of raster setting and fan speed, and scaled with counting statistics between 5 and 10 μA, which also confirms that the fluctuations at higher beam currents are target-related effects.
- Data taken under the same beam/target/raster conditions, but with different settings for the detector HVs (*e.g.*, runs 2259, 2260), showed that the detector widths were largely independent of high voltage, and that the electronic noise was small compared to the widths. The measured electronic noise (width of the ADC pedestals) was typically 13 channels (with OS=3, Low Gain setting on the ADC); with typical ADC peak values maintained around 40,000 channels, this electronic noise contributes about 230 ppm to the measured widths; added in quadrature this has little effect, except when the fluctuations were already small. The effect was confirmed by comparing results from several pairs of runs with different Lumi high voltages, but other conditions identical (*e.g.*, runs 2220, 2221).
- The comparison of the results from the three independent Lumi detectors gives additional confidence in the result, and a measure of our systematic errors.
- The present results were in good agreement with earlier parasitic studies done in Hall A in June and October 2002 [6].

9 Conclusions

1. The 30 Hz fluctuations observed for the machined-style cells at reasonable beam currents are unacceptable for the HAPPEX-II experiment; *e.g.* the 15 cm cell with the 2.8 mm×2.8 mm raster and 60 Hz fan speed exhibited 12,000 ppm fluctuations at 100 μA. Increases in raster area and target fan speed reduce the fluctuations somewhat, but are not sufficient to allow us to run with this target at anywhere near the planned beam current. Fluctuations are reduced for the 4 cm lH2 cell, but still become large above 40 μA.
2. The fluctuations can be large when the bulk effect is modest. The 15 Hz fluctuations, as measured by the widths of the 'asymmetry' distribution, are a *much more sensitive indicator of the onset of target density changes* than changes in the average luminosity.

3. The fluctuations have a time scale of order 100 ms, and are much smaller (maybe statistical?) at the 2 ms time scale. They are slow on the scale of the expected rate of fluid replacement in the raster volume. This may be important information for diagnosing the origin of the fluctuations. It also indicates that the target density probably does not respond to rapid changes in beam intensity *i.e.* at 30 Hz, so the effect of beam current asymmetry on the instantaneous target density will likely be somewhat damped out.

4. Orienting a rectangular (aspect ratio 2.7:1) raster vertically or horizontally had almost no effect on the boiling; the orientation of the raster with respect to the nominal fluid flow direction is not important.

5. Increasing the intrinsic beam spot by an order of magnitude had marginal effect on the fluctuations; the raster area and fan speed are much more important factors.

6. The present cells exhibit much worse behaviour for both fluctuations and the bulk effect than the experience from HAPPEX-I, which used 'beer can' cells.

7. For a given target fluid, the fluctuation widths scale crudely with the relative luminosity (bulk effect); the scaling is different for lD_2 than for lH_2. The fluctuations are *not* a simple function of the beam power per unit area; changing the raster area does not have the same effect as changing the beam current for constant power density.

8. Under similar conditions, the bulk effect and fluctuations are both about a factor of two smaller for lD_2 than for LH_2, with the fluctuations being somewhat smaller for a given fractional loss in overall density for lD_2 than for lH_2.

The present results have led us to decide that the HAPPEX-II experiment will use either 20 cm 'race-track' style transverse-flow target cells, which we expect to have improved flow characteristics, especially near the target windows, or, as a backup, the same 15 cm 'beer can' cell used in HAPPEX-I.

We plan on performing a very similar study with the racetrack and 'beer can' cell designs when HAPPEX-II takes data.

A Appendix: Summary of other Boiling studies

A.1 Bulk Effect

Table 2 shows the bulk effect results we have been able to gather from other measurements at JLab, and is almost certainly not exhaustive. In some cases, not all the details of the measurements were available to us, so one should take great care in comparing the results. In particular, it is not always clear if a raster value was given as setpoint or measured width at the target. Nevertheless, it is clear that the bulk effect slopes we have observed are not inconsistent with other data. Note that the data from Ref. [7] showed that the bulk effect scaled well with raster width, not raster area; also, note that the smaller slopes seen in the 1997 data compared to the 1996 data may have been due to a change made to the internal flow diverters. Finally, note that in all cases except [7], indications are that the reductions in density are larger for lH_2 than for lD_2, under similar conditions.

Target	Raster (mm $\times$ mm)	Fan Speed (Hz)	Slope $(100\mu A)^{-1}$	Reference
lH_2, 4 cm ‘beer can’	1.1 $\times$ 1.1	60	-7 %	Hall C, 1996 [7]
lD_2, 4 cm ‘beer can’	2.0 $\times$ 2.0	60	-4 %	Hall C, 1996 [7]
lD_2, 4 cm ‘beer can’	2.4 $\times$ 2.4	60	-3 %	Hall C, 1996 [7]
lD_2, 4 cm ‘beer can’	2.0 $\times$ 2.0	67	-2.4%	Hall C, 1997 [7]
lD_2, 12 cm ‘beer can’	2.0 $\times$ 2.0	67	-2.3%	Hall C, 1997 [7]
lH_2, 4 cm ‘beer can’	2.0 $\times$ 2.0	67	-1.1%	Hall C, 1997 [7]
lH_2, 4 cm ‘beer can’	2.0 $\times$ 2.0	40	-3.2%	Hall C, 1997 [7]
lH_2, 15 cm ‘beer can’	3.4 $\times$ 2.8	?	-5 %	Hall A, 1997 [8]
lD_2, 15 cm ‘beer can’	3.4 $\times$ 2.8	?	-3 %	Hall A, 1997 [8]
lD_2, 4 cm ‘tuna can’	2.0 $\times$ 2.0	60	-2.4 %	Hall C, 1999 [9]
lH_2, 15 cm ‘cigar tube’	2.0 $\times$ 2.0	60	-19 %	Hall C, 2001 [10]
lD_2, 15 cm ‘cigar tube’	2.0 $\times$ 2.0	50	-10 %	Hall C, 2001 [10]
lD_2, 4 cm ‘cigar tube’	2.0 $\times$ 4.0	60	-7.2 %	Hall C, 2000 [10]
lD_2, 4 cm ‘cigar tube’	2.0 $\times$ 4.0	60	-7.4 %	Hall C, 2000 [10]
lD_2, 15 cm ‘cigar tube’	2.0 $\times$ 4.0	60	-12 %	Hall A, 2002 [11]

Table 2: Bulk effect slopes: % change in apparent luminosity for a beam current change from 0 to 100 μA, from other JLab cryotarget studies.

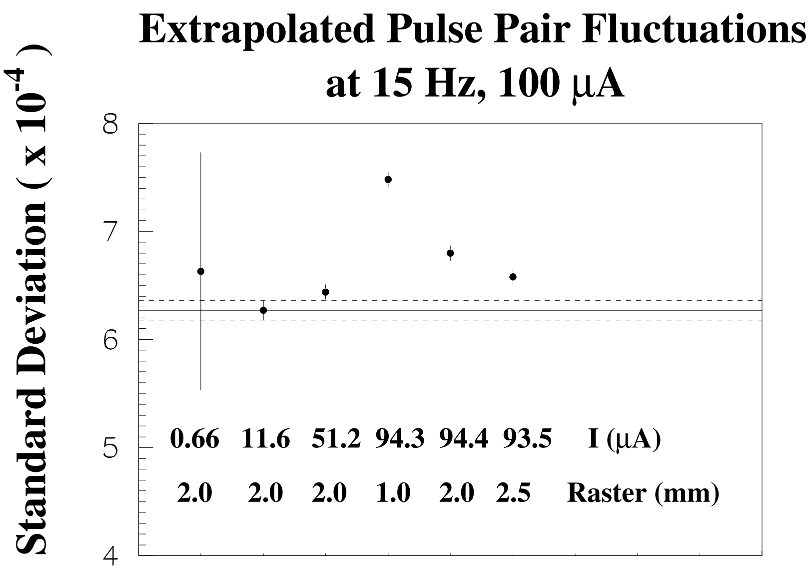

Figure 42: HAPPEX-I Boiling results. The results are normalized to the σ one expects for a beam current of 100 μA, assuming counting statistics. As a reference, the horizontal line indicates the measured result at 11.6 μA, as an estimate of the pure counting statistics value.

A.2 Fluctuations

Pioneering studies on target fluctuations for a parity experiment were done by the SAMPLE collaboration [12]. Their 40 cm long lH_2 target cell has primarily longitudinal fluid flow. Comparisons of the widths of the detected asymmetry distributions for various repetition rates and average beam currents showed no significant increase in the width beyond counting statistics ($\sim$ 3500 ppm). An upper limit of target density fluctuations at 30 Hz was set at $<$ 1000 ppm.

HAPPEX-I studied target fluctuations directly in a test run in October 1997 [2]. At a lower beam energy (925 MeV) and a 12.8° scattering angle, the elastic scattering rate from hydrogen was of order 50 MHz at 100 μA, leading to narrow counting statistics widths of order 620 ppm for the focal plane detectors (compared to 3,600 ppm for the kinematics of the main experiment). The cell used was a 15 cm lH_2 'beer can' cell. The raster was square, and the target fan speed was 70 Hz. By varying beam current and raster size, it was determined that the fluctuations were $\sim$200 ppm at 95 μA with a 2 mm$\times$2 mm raster; see Fig. 42 and Table 3.

During the 1998 HAPPEX-I run, no significant increase in the detector widths due to target density fluctuations were seen; typically, the raster size was 1.4 mm$\times$1.7 mm, and the target fan speed was 72 Hz.

During the 1999 HAPPEX-I runs, which ran at reduced beam current (30-50 μA), fluctuations were observed on occasion, partly due to problems with interactions between the beam tune and the raster size, and the use of a 'circular' raster which was somewhat non-uniform. Typically, when a larger spot size was used (5 mm$\times$5 mm), the fluctuations were unobservably small; see Table 3.

At SLAC, the E158 experiment (parity violation in Møller scattering), uses a very different target design [14], similar to the SAMPLE target in concept. With a 1 mm rms radius beam, on a 1.5 m long lH_2 target, and with a 120 Hz repetition rate and 6×10^{11} electrons/pulse, they were able to set an upper limit on fluctuations of 65 ppm.

The G^0 experiment in Hall C at JLab uses a target with similar design concept to the E158 target; results from the commissioning run in the Fall of 2002 showed that at 40 μA, with a 2.2 mm$\times$2.2 mm raster, fluctuations were 119 ppm (see Table 3) at the nominal fan speed (30 Hz); they were reduced to 49 ppm at the maximum speed of 42 Hz and increased to 410 ppm at 19 Hz fan speed. In comparison with the present results with the Hall A cryotarget with the 'cigar tube' cells, the G^0 target exhibited fluctuations more than an order of magnitude smaller for similar beam power density.

References

[1] K.A. Aniol *et al.*, Phys. Rev. Lett. **8**, 1096 (1999); K.A. Aniol *et al.*, Phys. Lett. B **509**, 211 (2001).

[2] G.A. Rutledge, 'Measurement of the Strange Sea of the Proton', PhD thesis, College of William & Mary, (2001) (unpublished) [http://physics.wm.edu/~armd/GRutledge_thesis.pdf].

[3] JLab experiment E99-115, Spokespersons K. Kumar and D. Lhuillier.

[4] Mikell Seely, 'Global and Local Beam Heating Revisited' (unpublished technical note) 9/16/2002.

[5] G.W. Miller, 'Parity Violation in Forward Angle Elastic Electron-Proton Scattering', PhD thesis, Princeton U., (2001) (unpublished) [http://www.jlab.org/~humensky/ParityExpts/DOCS/Thesis_Wilson.ps.gz].

[6] Riad Suleiman, 'Beam Test Results of the Luminosity Monitor for Hall A Parity Experiments', July 2002, (unpublished) [http://www.jlab.org/~suleiman/Lumi/lumi_talk.ps]

Target	Raster (mm × mm)	Current (μA)	Power Density (μA/(mm^2))	Fluctuations (ppm)	Reference
40 cm	3 × 3	40	4	$\leq$ 1000	SAMPLE, 1996 [12]
15 cm, 'beer can'	2.5 × 2.5	94	15	200	HAPPEX-I, 1997 [2]
15 cm, 'beer can'	2.0 × 2.0	94	24	250	HAPPEX-I, 1997 [2]
15 cm, 'beer can'	1.0 × 1.0	94	94	400	HAPPEX-I, 1997 [2]
15 cm, 'beer can'	2.0 × 2.0	51	13	$\leq$ 125	HAPPEX-I, 1997 [2]
15 cm, 'beer can'	5.0 × 5.0	47	2	$\leq$ 100	HAPPEX-I, 1999 [13]
15 cm, 'beer can'	2.0 × 2.0	47	12	1000	HAPPEX-I 1999 [13]
15 cm, 'beer can'	1.5 × 1.5	47	21	1250	HAPPEX-I, 1999 [13]
140 cm	1.0 × 1.0	11	11	$\leq$ 65	SLAC E158, 2002 [14]
20 cm	2.2 × 2.2	40	8	119	G^0, 2002 [15]
20 cm	2.2 × 2.2	30	6	57	G^0, 2002 [15]
20 cm	2.2 × 2.2	20	4	37	G^0, 2002 [15]

Table 3: Other measurements of 15 Hz density fluctuations in lH_2 targets.

[7] Kenneth Gustafsson, 'Measurement of Deuteron Tensor Polarization in Elastic Electron Scattering', PhD thesis, U. Maryland, 2000; (appendix B) [http://www.physics.umd.edu/enp/theses/].

[8] Kathy McCormick, (October, December 1999), PhD thesis, Old Dominion U. (1999) (unpublished); private communication.

[9] Eric Christy, E94-110 data (July, August 1999), private communication, [http://www.jlab.org/Hall-C/talks/01_09_03/Smith.pdf].

[10] Greg Smith, (Summer 2000, April 2001), private communication, [http://www.jlab.org/Hall-C/talks/01_09_03/Smith.pdf].

[11] Eric Voutier, HALOG entry 88696, Oct. 21 2002, [http://www.jlab.org/~adaq/halog/html/0210_archive/021021224128.html].

[12] E.J. Beise *et al.*, Nucl. Instrum. Methods **A 378**, 383 (1996).

[13] Robert Michaels, HALOG entry 22223, July 10 1999, [http://hallaweb.jlab.org/adaq/log/html/9907_archive/990710130911.html].

[14] J. Gao *et al.*, 'A Liquid Hydrogen Target for the Precision Measurement of the Weak Mixing Angle in Møller Scattering at SLAC' , submitted to Nucl. Instrum. Methods, 2002.

[15] Silviu Covrig, private communication (April 2003).